Blanco-Alegre C., Fialho P., Calvo A.I., Castro A., Coz E., Oduber F., Prévôt A.S.H., Močnik G., Alves C., Lucarelli F., Nava S., Calzolai G., Fraile R. (2022) Contribution of coal combustion to black carbon: coupling tracers with the aethalometer model. Atmospheric Research, 267, 105980.

The final publication is available at https://doi.org/10.1016/j.atmosres.2021.105980

Contribution of coal combustion to black carbon: coupling tracers with the aethalometer model

C. Blanco-Alegre[1], P. Fialho[2], A.I. Calvo[1], A. Castro[1], E. Coz[3], F. Oduber[1], A.S.H. Prévôt[4], G. Močnik[5,6], C. Alves[7], F. Giardi[8], G. Pazzi[8], R. Fraile[1]

[1]Department of Physics, IMARENAB University of León, 24071 León, Spain
[2]Institute of Volcanology and Risk Assessment – IVAR, Rua da Mãe de Deus, 9500-321 Ponta Delgada, Portugal
[3]Centre for Energy, Environment and Technology Research (CIEMAT), Department of the Environment, Madrid, Spain
[4]Laboratory of Atmospheric Chemistry, Paul Scherrer Institute, 5232 Villigen, Switzerland
[5]Center for Atmospheric Research, University of Nova Gorica, 5270 Ajdovščina, Slovenia
[6]Condensed Matter Physics Dept., Jožef Stefan Institute, 1000 Ljubljana, Slovenia
[7]Centre for Environmental and Marine Studies (CESAM), Department of Environment and Planning, University of Aveiro, Aveiro 3810-193, Portugal
[8]Department of Physics and Astronomy, Università di Firenze and INFN-Firenze, 50019 Sesto Fiorentino, Italy

Corresponding Author: aicalg@unileon.es *+34987291543*

ABSTRACT

Black carbon (BC) aerosol characteristics have been analysed from January 2016 to March 2017 in an urban background area (León, Spain), located in a coal-mining region, where this fuel is commonly used. The monthly and seasonal variations of BC and source contributions were examined. The mean equivalent BC concentration (eBC) during cold and warm months were 1.0±0.5 and 0.6±0.2 μg m^{-3}, respectively. eBC can be further divided into eBC_{ff} (eBC from liquid fossil fuel) and eBC_{bb+cc} (eBC from biomass burning plus coal combustion), with mean annual values of 0.6±0.3 and 0.3±0.3 μg m^{-3} (cold months) and 0.4±0.2 μg m^{-3} and 0.1±0.1 μg m^{-3} (warm months), respectively. The eBC obtained from the aethalometer and the elemental carbon (EC) quantified through a Thermal Optical Transmittance method presented a significant strong positive correlation in both warm (r=0.82) and cold (r=0.88) periods. A mass absorption cross-section (MAC) of 4.46±0.16 between two techniques has been obtained. In the cold period, a multilinear regression model to decouple eBC_{bb} from eBC_{cc} was established (r^2=0.85) based on two tracers: arsenic for coal combustion and potassium for biomass burning. The model application enabled us to distinguish the contributions to eBC_{bb+cc} (as a function of the variance explained by the tracers) in the cold period: 74% from biomass burning and 26% from coal combustion. The highest eBC_{cc} concentration was estimated for December 2016 and January 2017 (0.18 μg m^{-3}). This result was supported by the Absorption Ångström Exponent (AAE), which showed the maximum value in January 2017 (1.43±0.37) due to the high biomass burning and coal combustion contributions.

KEYWORDS: absorption coefficient, coal-mining, equivalent black carbon, meteorological variables, seasonal pattern.

1. INTRODUCTION

One of the main risks to human health and climate change is air pollution. According to the World Health Organisation (WHO) estimates, approximately 90% of the population breathes polluted air. The areas with the highest levels of pollution, caused by gases and particulate matter, are the Eastern Mediterranean Region and South-East Asia (WHO, 2013).

Black carbon (BC) is one of the most important components of atmospheric particulate matter; it is a short-lived climate pollutant released from incomplete combustion processes of fossil fuel and biomass. It has several distinctive physical properties: it strongly absorbs visible light, it is refractory and insoluble in water and many organic solvents, and it exists as an aggregate of small spherules (Bond et al., 2013). The main sources of BC are: i) diesel engines used for transport, ii) residential solid fuels (wood and coal), iii) forest fires and iv) industrial processes (Bond et al., 2013). The BC concentration depends on the source contributions and the atmospheric conditions. A clear relationship between eBC concentration and meteorological parameters has been reported by several authors (Kucbel et al., 2017; Meena et al., 2021; Shen et al., 2021; Tan et al., 2020), who observed higher eBC concentration with the decrease in wind speed and the increase in relative humidity. Another important factor is the atmospheric boundary layer (ABL) height, which controls the BC concentration at surface level (Huang et al., 2018; Ji et al., 2017; Joshi et al., 2016; Shen et al., 2021) during the whole year. The atmospheric lifetime of BC ranges from days to weeks and its main sinks are wet and dry deposition (Begam et al., 2016). Blanco-Alegre et al. (2019) have found a decrease of 40% in BC concentration after rain events in León, Spain.

Recent studies on BC health risks indicate that together BC and organic carbon may contribute to around 3 million premature deaths every year (Apte et al., 2015; Bond et al., 2013; Lelieveld et al., 2015; WHO, 2012). Other studies also relate short-term BC exposure to pulmonary inflammation and asthma-related effects (Saenen et al., 2016). The other great impact of BC is its effect on climate inasmuch as BC strongly absorbs solar radiation and can act as cloud and ice nuclei. BC is the second strongest contributor to current global warming, after CO_2, with an estimated global mean radiative forcing between 0.4 and 1.2 W m^{-2} (ICCP, 2014). Other effects are lower atmospheric visibility and plant growth stunting (Auffhammer et al., 2006; Chameides et al., 1999). Therefore, studying BC is critical due to its multiple effects on climate, public health and air quality (EEA, 2016; Kinney, 2008; Tong et al., 2017, 2016). An example of this is the high number of publications about BC in the past few years (Blanco-Alegre et al., 2021; Kang et al., 2020), with important advances in the knowledge of BC characteristics and its impacts (Chen et al., 2020; Dumka et al., 2018; Tan et al., 2020; Wu et al., 2018; Yang et al., 2019).

The aethalometer (Hansen et al., 1984) has become an instrument widely used to quantify BC. It measures the aerosol light attenuation (at wavelengths from near-ultraviolet to near-infrared) and determines the equivalent BC (eBC) (Andreae and Gelencsér, 2006; Petzold et al., 2013) by using the specific mass attenuation cross-section reported in the manufacturer manual, for the working wavelengths. The wavelength dependence of the determined absorption coefficient was used to estimate the contribution of the main sources to eBC, fossil fuel (eBC_{ff}) and biomass burning (eBC_{bb}) using the so-called Aethalometer model (Sandradewi et al., 2008a) approach. This approach can be applied whenever the presence of iron oxides is not foreseen (iron oxides are also responsible for enhancement in the UV and visible wavelengths (Fialho et al., 2014) and result in wrong estimations given by the Sandradewi et al. (2008a) approach).

The Aethalometer model was developed in an area with no influence of coal sources and only considers the presence of two major sources of BC: biomass burning and fossil fuel (associated with traffic). Following Harrison et al. (2013), this approach needs improvement for areas where the presence of other sources, such as coal combustion, cannot be neglected. Information on the contribution of coal combustion to eBC is still scarce. The fact that coal smoke absorbs at the shortest wavelengths as biomass smoke (Bond et al., 2002; Harrison et al., 2013) constitutes a major problem in estimating the contribution of each source to the eBC, by using only the aethalometer measurements. Thus, in regions where coal combustion is a common practice, the Sandradewi et al. (2008a) approach can be improved by adding other types of measurements, as Herich et al. (2011) have previously shown.

It has to be emphasised that Absorption Ångström Exponent (AAE) values for coal combustion can be very variable, from close to 1 to nearly 3 (Bond, 2001), depending on the type of coal and combustion technology (Harrison et al., 2013). For biomass, AAE values also vary with biomass type and combustion condition (Garg et al., 2016; Pokhrel et al., 2016; Xie et al., 2018). However, in other studies the values for traffic (around 1.0) and for biomass (around 1.5-2) are much more delimited (Kirchstetter et al., 2004; Tobler et al., 2020; Zotter et al., 2017).

The importance of BC source apportionment studies lies in the fact that coal and residential biomass burning are the main emission sources (between 60-80%) of this carbonaceous component, not only in Africa and Asia (Bond et al., 2013), but also in European cities with coal power plants (Kucbel et al., 2017). In 2010, in Europe, residential combustion of solid fuels (biomass and coal) for heating accounted for 13-21% of the total ambient $PM_{2.5}$ emissions (WHO/United Nations, 2018). Thus, the methodology to estimate the contribution of coal combustion to eBC would be very useful in areas such as the city of León, Spain, where the use of coal in domestic heating devices is still widespread. China or southern Poland are other examples where this practice has become one of the most polluting activities. Along with other contaminants, high emissions of elements such as fluorine, arsenic, selenium, mercury and lead may have significant global repercussions and be particularly harmful to human health

(WHO/United Nations, 2018). Evidence of this is that some authors have already found a relation between coal combustion and mortality in Beijing (Tang et al., 2017).

The main aim of this paper is to characterise the eBC sources during a 14-month sampling campaign in León, a city located in a coal-mining region, in the NW of the Iberian Peninsula. The annual and seasonal evolution of this pollutant was studied and the contribution for its three main sources (traffic, coal combustion and biomass burning) was quantified. To achieve this purpose, a methodology to decouple the eBC contribution of coal combustion and biomass burning is established during the cold period. This work represents a step forward in the quantification of eBC from different sources and the method developed can be very useful in regions where coal combustion, biomass burning and traffic are the main BC sources. In addition, this study provides new information for air quality models, which need new metrics in Europe to implement actions that reduce BC concentrations.

2. MATERIAL AND METHODS

2.1. Sampling site

Sampling was conducted between 2 January 2016 and 31 March 2017 at the campus of the University of León (León, Spain) (Figure A1). In total 346 days were covered, but only 327 were fully studied due to sampling problems. León is a city located in the NW of the Iberian Peninsula (42° 36′ N, 05° 35′ W at 838 m a.s.l.) with a population of about 200,000 inhabitants (population density close to 3300 people km^{-2}) (INE, 2017). According to the Spanish Meteorological Office (http://www.aemet.es/en/), in the past 35 years, an annual mean precipitation of 515 mm and a temperature of 11.1 °C were registered. In the city, along the whole year, the main sources of particulate emissions identified by Positive Matrix Factorization six-factor solution, were: traffic (29%), aged sea salt (26%), secondary aerosols (16%), dust (13%), marine aerosol (7%) and biomass burning (3%) (Oduber et al., 2021). The traffic density can be considered medium compared with other Spanish cities, concentrated mainly on the ring road that surrounds the city (~250 m northeast from the sampling point), with an average daily vehicle intensity of 25,000 vehicles day^{-1}. The vehicular fleet is composed by 44% vehicles powered by gasoline and 56% by diesel (DGT, 2016). Furthermore, biomass (mainly oak and beech) and coal burning for residential heating are common in the cold months. Oduber et al. (2019) reported a decrease of 2.35 µg m^{-3} $year^{-1}$ in PM_{10} levels in the past 19 years in this city, mainly due to the environmental policies adopted. In the past 10 years, the city presented an average PM_{10} concentration of 20.0±5.0 µg m^{-3} (Junta de Castilla y León, 2018).

In 2016, 476 tonnes of BC were emitted in the province of León (IDAE, 2017). The sectors with the highest BC emission were non-industrial combustion plants (55%), waste treatment and disposal (15%), road transport (14%), other types of transport and road-mobile machinery (10%), industrial combustion (4%) and combustion for the production and transformation of energy (2%) (Spanish Ministry for Ecological Transition, 2018). In León, the total heat demand is 1.6×10^6 MW h year^{-1} (IDAE, 2017). Regarding heating devices, the main energy sources are gas-oil (29%), gas (28%) and electrical (11%), followed by biomass burning (6%) and coal combustion (6%) (Junta de Castilla y León, 2008). The León mining zone is constituted by anthracite and hard coal deposits, with a high carbon content (>75%) (Junta de Castilla y León, 2009), but a significant fraction of the coal used is imported (~85%), mainly anthracite from Russia.

2.2. Methodology

2.2.1. Black carbon

Aerosol light-attenuation at seven wavelengths (370, 470, 520, 590, 660, 880 and 950 nm) was continuously measured with an aethalometer, model AE-31 (Magee Scientific, USA) equipped with an Extended Range chamber and a PM_{10} inlet without pre-drying the sample. The sampling flow rate was set at 4 L min^{-1}, and measurements were taken every 2-minutes. To reduce data noise 10-minutes and 1-hour averages were calculated. A detailed description of the instrument can be found in Fialho et al. (2005) and Hansen (2005).

The eBC data recorded during the sampling period were corrected following WMO/GAW Aerosol Measurement Procedures, Guidelines and Recommendations (WMO, 2016). Aethalometer data were also corrected for the loading effect (Figure A2) by using the Weingartner et al. (2003) algorithm with the winter campaign parameters for cold months and with the summer campaign parameters for warm months (TableA1) proposed by Sandradewi et al. (2008b). The 470 nm (α_1) and 950 nm (α_2) wavelengths were used to estimate hourly eBC, eBC_{ff}, eBC_{bb} concentrations and AAE (Sandradewi et al., 2008a) (see Appendix). The AAE specific values used to discriminate between fossil fuel and biomass burning contributions were $AAE_{ff}=1.0$ and $AAE_{bb}=1.68$ (Zotter et al., 2017). Anomalous AAE data recorded every 2-minutes (those below 0.7 and above 5) were discarded as these measurements are not indicative of real eBC. These values were selected based on the probability density function (pdf) of the AAE values (Figure A3). The discarded data account for less than 1% in the sampling period.

As mentioned above, coal combustion can become an important contributor to eBC during the cold period in León. It is expected that eBC attributed to biomass burning also includes eBC from coal combustion (eBC_{bb+cc}) (Bond et al., 2002; Harrison et al., 2013) and we have used the same AAE of 1.68 for both of them, since it is the combustion efficiency which controls the optical properties rather than the type of fuel. To achieve the aim of estimating the coal combustion (eBC_{cc}) fraction from eBC_{bb+cc}, a model was developed by considering the linear regression between the eBC_{bb+cc} with biomass and coal combustion tracers.

2.2.2. Carbonaceous aerosols

A high-volume air sampler (CAV-A/Mb model) equipped with a PM_{10} inlet head and 150 mm diameter quartz filters was used to collect the aerosol in the air flow for carbon analysis. Each filter sampled for a period of 23.5 h (≈ 1 day, from 1200 UTC to 1130 UTC the following day) and the mass content was determined by gravimetric methods. Total carbon (TC) mass was obtained by the Thermal Optical Transmittance method (TOT). To discern between EC and OC, the sample was first heated to 600 ºC in a N_2 atmosphere to vaporise the organic fraction of aerosol particles. Then, EC was determined by sequential heating at 850 ºC in an atmosphere containing 4% O_2. Correction for the pyrolysis contribution to EC from OC was carried out by controlling the transmission of light across the filter with the laser beam. The distinction between OC and EC was completed when the transmittance reached the initial value. A detailed description of the technique and equipment used have been outlined in Pio et al. (2011) and Castro et al. (1999), respectively. A global scheme of the methodology to split OC/EC carried out in Aveiro, Portugal, can be seen in the European report about measurement of EC and OC in Europe (Kuhlbusch et al., 2009).

2.2.3. Major tracers

A low volume sampler (TECORA ECHOPM) equipped with a PM_{10} inlet head collected aerosol on teflon filters (47 mm diameter) for 23.5 h periods (≈ 1 day), later used in PIXE (Particle-Induced X-ray Emission) for major and trace element analysis, following the methodology described by Lucarelli et al. (2014). These daily samples were also analysed using ionic chromatography coupled with pulsed amperometric detection (Gonçalves et al., 2021) to obtain levoglucosan concentrations. The estimated uncertainties for the ion chromatography and PIXE measurements depend on the element analysed and its detection limit. These uncertainties ranged from 2% to 14% during the sampling campaign.

2.2.4. Meteorological parameters

A weather station was used to record temperature (T), relative humidity (RH), pressure (P) and wind speed (WS) and direction. The last two variables have been used as input data for *polar plots* (Carslaw, 2015; Carslaw and Ropkins, 2012). Furthermore, ABL height, which controls the eBC concentration at ground level (Heintzenberg et al., 2016), was obtained from the National Oceanic and Atmospheric Administration (NOAA). The meteorological data used were provided by Global Data Assimilation System (GDAS), with a spatial resolution of 1 degree and a temporal resolution of 3 hours. A good correlation between ABL heights from GDAS forecasts and from LIDAR measurements has been reported by Moreira et al. (2020). Due to the importance of WS (m s^{-1}) and ABL (m) variables in the dispersion of pollutants (Moreira et al., 2020; Zhu et al., 2018), the so-called ventilation coefficient (VC; m^2 s^{-1}), has been calculated. Because of the temporal resolution of available ABL data, the VC was estimated every 3 h. Consistent with meteorological variables and the use of heating devices, the year was divided into two periods: cold period, from September 15 to April 14, and warm period, from April 15 to September 14.

2.2.5. Statistical analyses

A univariate analysis (i.e. mean, minimum, maximum and standard deviation) and bivariate Pearson correlations with 95% confidence intervals have been used to characterise eBC in León. Through the Pearson correlations, the linear association, direction, and strength of the relationships between eBC, air pollutants and meteorological variables have been determined. The strength of the correlation (significant over 0.1 for 10455 hours of sampling) was classified according to the following positive or negative correlation ranges: <0.1 no correlation, 0.1-0.3 weak, 0.3-0.5 moderate, 0.5-0.7 strong, and >0.7 very strong correlation.

To characterise the days according to the concentration of pollutants, a two-stage cluster classification was performed. Details will be presented in section 3.2.2.

3. RESULTS AND DISCUSSION

3.1. General overview

In the following subsections, after the application of the Aethalometer model (Sandradewi et al., 2008a), we describe the evolution of eBC and AAE, the relation of eBC with meteorological conditions and the results of the thermal optical transmittance method.

3.1.1. Evolution of eBC

After applying the Aethalometer model, and once the contribution of each source to the eBC (eBC_{ff} and eBC_{bb+cc}) was known, a seasonal analysis was carried out.

A mean hourly eBC mass concentration of 0.9±0.9 µg m^{-3} was obtained for the sampling campaign. By seasons, the highest concentration was registered in winter 2017 (1.1±0.6 µg m^{-3})

and autumn (1.1±0.5 μg m^{-3}), followed by winter 2016 (0.9±0.4 μg m^{-3}), summer (0.6±0.3 μg m^{-3}) and spring (0.6±0.2 μg m^{-3}). León is characterised by the absence of large manufacturing activities compared to other industrialised cities, but with a regular use of coal combustion in domestic heating devices (Junta de Castilla y León, 2009). As can be seen in Table A2, the locations with eBC concentrations similar to León like Rotterdam (0.8±0.5 μg m^{-3}), Amsterdam (1.4±0.6 μg m^{-3}) (Klompmaker et al., 2015), Montreal (1.1±1.3 μg m^{-3}) (Weichenthal et al., 2014) and Valparaiso (0.8-0.9 μg m^{-3}) (Marín et al., 2017) present more inhabitants and larger industries than León. In the Mediterranean area, in Athens, Greece, Liakakou et al. (2020) reported a higher mean annual eBC concentration of 1.9±2.5 μg m^{-3}. Compared to other Spanish cities of similar population, the concentration in León was lower than that recorded in a winter campaign in Granada, both in suburban (2.9±3.0 μg m^{-3}) and urban (3.0±3.0 μg m^{-3}) areas (Casquero-Vera et al., 2021). This fact may be caused by the frequent stagnant conditions in this city (Lyamani et al., 2012). Based on a one-year sampling period, Santa Cruz Tenerife (0.8±0.4 μg m^{-3}) and Huelva (0.7±0.4 μg m^{-3}) presented similar eBC concentrations due to a reduced impact of traffic in smaller cities. However, Barcelona with a larger population and more traffic presented a higher eBC concentration (1.7±0.6 μg m^{-3}) than León (Reche et al., 2011).

In Figure 1, eBC concentrations are plotted throughout the sampling period, with a time resolution of 10 minutes. In winter, high values are reached, probably due to residential biomass burning and coal combustion. It is worth noting that the highest eBC values were registered in January 2017 when compared to January 2016. This was probably a consequence of the lower mean temperature recorded in January 2017 (on average, 2 °C less than in January 2016). The dynamics of the atmospheric boundary layer height may also have played an important role. In autumn and winter, the ABL height is lower, preventing the dispersion of pollutants (Joshi et al., 2016), particularly in October, November and December 2016. The correlation between ABL height (at 0000, 0300, 0600, 0900, 1200, 1500, 1800 and 2100) and daily eBC concentrations has been determined. A significant statistical negative correlation all year round has been obtained (Table A3), but the link was especially strong in autumn and winter, when the ABL height was lower. The time frame with a major influence of the ABL on the eBC concentrations was between 0900 and 1800 (highest values of Pearson correlations), with a maximum influence at 0900. Besides, these time periods coincide with rush hours. The lowest ABL heights at 0900 were registered in winter and autumn (424±356 and 229±219 m, respectively), while in spring and summer values of 695±223 and 573±164 m, respectively, were recorded. The pivotal role of ABL height in the dilution of eBC concentrations has been observed in other cities, such as Pune, India, with eBC concentrations between 0.6 and 13.1 μg m^{-3} (Meena et al., 2021), or Athens, Greece, mainly with ABL heights lower than 500 m (Liakakou et al., 2020).

The evolution of VC along the day showed a clear rise of VC at 1200 and 1500 UTC (Table A4) with values between 1145.0 $m^2 s^{-1}$ at 1200 UTC in autumn and 3500.5 $m^2 s^{-1}$ at 1500 UTC in summer. As observed by Moreira et al. (2020) in Granada, Spain, with similar VC values, a pattern was registered characterised by the lowest concentrations of eBC in all seasons during central hours, in line with the highest values of VC.

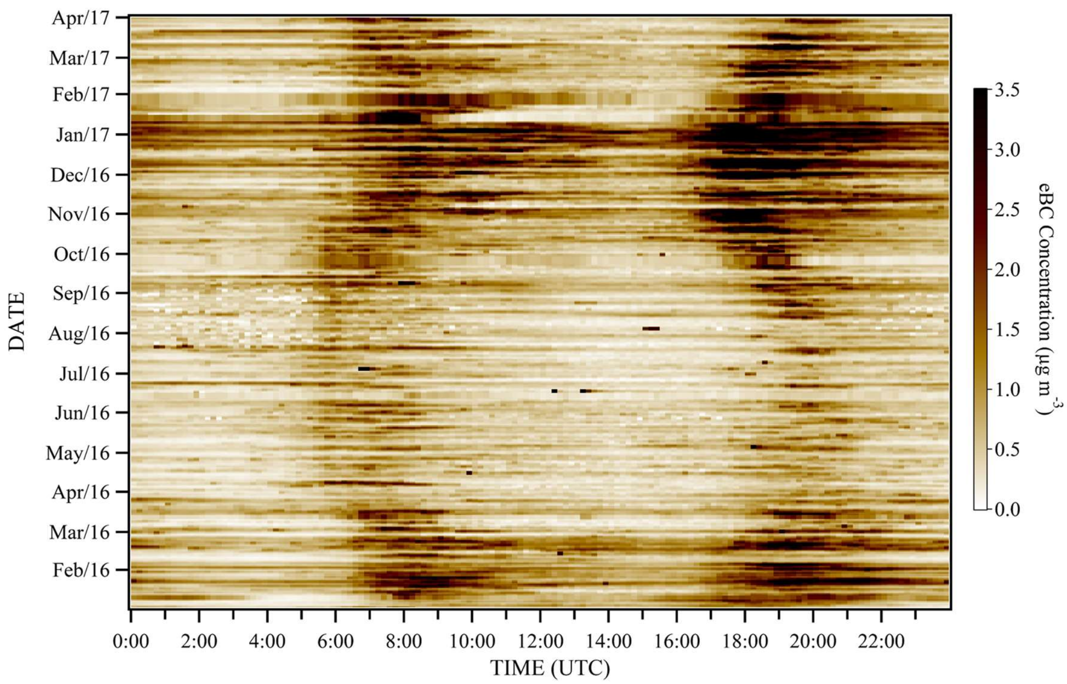

Figure 1. Temporal variations of eBC concentration (colour code) measured at León between January 2016 and March 2017.

It should be noted that the sporadic points observed in Figure 1 with high concentrations in summer months are probably due to the occurrence of small fires - sometimes stubble burnings-, which are still very common in the area near the sampling point (Lucas-Borja et al., 2016). These activities contributed to the high concentrations of eBC in the atmosphere of León, corroborated by the increase in the levels of potassium (as will be seen in section 3.2.1), a biomass burning tracer (Herich et al., 2011; Pachon et al., 2013).

3.1.2. Aethalometer model application

The month with the highest eBC mean concentration was December 2016 with 1.6±0.6 µg m^{-3}, value about 3 times higher than the lowest (0.5±0.1 µg m^{-3}), registered in April 2016 (Table 1). The monthly maximum AAE (1.43±0.37) was reached in January 2017, corresponding to the maximum eBC_{bb+cc} concentration (0.67±0.41 µg m^{-3}). In contrast, the monthly minimum AAE (1.23±0.46) was recorded in June 2016 when the minimum eBC_{bb+cc} concentration (0.12±0.24 µg m^{-3}) was observed. AAE and eBC values were mainly associated with road traffic emissions (the low eBC values in the summer months result from the decrease in the number of vehicles in circulation due to the vacation period), the contribution of biomass and coal combustion in the cold period and the meteorological conditions (Table A3) such as thermal inversions (Gramsch et al., 2014; Lyamani et al., 2012). The seasonal maximum was reached in winter 2017 (1.37±0.10), while the minimum was registered in summer (1.26±0.08). The AAE in the warm period was higher than the AAE found by Tan et al. (2020) over the Yangtze River Delta in China, reporting a maximum of 1.35 during wintertime and 1.12 during summertime.

Table 1. Monthly mean values (± standard deviation) calculated for eBC, eBC_{ff} and eBC_{bb+cc}, interpolated Absorption Ångström Exponent obtained from 470 nm and 950 nm (AAE) and percentage of biomass burning plus coal combustion (BB+CC (%)).

Year	Season	Month	eBC (μg m^{-3})	eBC_{ff} (μg m^{-3})	eBC_{bb+cc} (μg m^{-3})	AAE	BB+CC (%)
2016	Winter	January	1.00±0.41	0.69±0.3	0.31±0.14	1.29±0.33	32±9
	Winter	February	0.94±0.47	0.62±0.29	0.31±0.20	1.30±0.36	32±7
	Spring	March	0.72±0.30	0.50±0.20	0.22±0.12	1.27±0.41	29±8
	Spring	April	0.49±0.13	0.35±0.11	0.14±0.04	1.31±0.47	29±7
	Spring	May	0.56±0.14	0.43±0.11	0.13±0.04	1.25±0.48	23±6
	Summer	June	0.53±0.20	0.41±0.14	0.12±0.11	1.23±0.46	22±8
	Summer	July	0.54±0.19	0.41±0.14	0.12±0.10	1.24±0.49	22±8
	Summer	August	0.61±0.20	0.48±0.16	0.12±0.05	1.26±0.54	20±3
	Autumn	September	0.80±0.33	0.58±0.21	0.22±0.15	1.3±0.5	27±8
	Autumn	October	0.98±0.31	0.73±0.24	0.24±0.11	1.25±0.36	25±6
	Autumn	November	1.10±0.52	0.72±0.34	0.38±0.19	1.31±0.33	34±7
	Winter	December	1.62±0.59	1.02±0.36	0.6±0.28	1.31±0.27	36±8
2017	Winter	January	1.50±0.81	0.83±0.54	0.67±0.41	1.43±0.37	44±14
	Winter	February	0.82±0.34	0.50±0.19	0.32±0.20	1.37±0.44	37±10
	Spring	March	0.79±0.34	0.46±0.18	0.33±0.22	1.37±0.42	39±12

As mentioned above, AAE values for coal combustion can be variable, ranging from values close to 1 to nearly 3 (Bond, 2001). Nevertheless, Sun et al. (2017) documented an AAE_{cc} of 1.30±0.32 for anthracite chunks coal, typically used in León, in stoves for raw-coal chunks. Thus, the emission from coal combustion can contribute to an increase in AAE in the cold period. Months with high biomass burning correspond to an AAE increase due to the emission of larger particles from this source (Russell et al., 2009; Alonso-Blanco et al., 2018).

3.1.3. Relationship between eBC and meteorological conditions

Pearson correlations (Table A5) indicated a significant negative correlation between eBC_{bb+cc} and temperature due to the use of heating devices, mainly in autumn and winter. Although moderate in the winter months, as for AAE, a weak negative correlation with temperature throughout the year was observed. Temperature explained 17% of the variance of AAE in December 2016. eBC_{ff} did not show a clear relationship with temperature because its main source was traffic, non-dependent directly on weather conditions. Thus, throughout the year, a significant weak negative correlation was registered.

A significant moderate negative correlation between wind speed and eBC has been observed throughout the year, as observed in other studies (Kucbel et al., 2017). Thus, under high wind speed conditions, eBC concentration decreases, due to intense pollutant dispersion, a pattern also observed e.g. in Pune and Mahabaleshwar, India, by Meena et al. (2021). Our study found that wind speed explained 21% of the variance of eBC_{ff} in March 2017.

For relative humidity, the variance explained of eBC_{ff} was less than 1% in all months, contrary to other studies (Kucbel et al., 2017; Meena et al., 2021; Tan et al., 2020) which observed higher eBC concentration during high RH conditions. Similar results have been reported by Shen et al. (2021), who observed that meteorological conditions influenced the concentration and distribution of eBC concentrations: increasing concentrations were registered when there was a decrease in wind speed and an increase in relative humidity. The study of the relationship between eBC and rainfall has been conducted by Blanco-Alegre et al. (2018) in León, who showed a different rain scavenging effect according to the eBC source. This fact was also observed in Athens, Greece, by Liakakou et al. (2020).

The mean ventilation coefficient (VC) during the sampling was 795.8 $m^2 s^{-1}$, being higher during the warm period (1010.5 $m^2 s^{-1}$ on average) than during the cold period (650.9 $m^2 s^{-1}$). Pearson correlations indicate a significant negative correlation between VC and eBC, eBC_{ff} and eBC_{bb+cc} during the whole sampling campaign. Thus, a better correlation between air pollutants and the VC has been observed than using only wind speed or ABL height.

eBC_{bb+cc} and eBC_{ff} concentrations showed dependence on wind direction and speed, as depicted in the polar plots (Fig. 2). In the cold period (autumn and winter), the eBC_{ff} mostly originated in quadrant III (between S and W), which coincides with the geographical location of the city centre. The contribution from I and II quadrants was mainly due to the León ring road. Likewise, the values of eBC_{bb+cc} were higher in the cold period, but in spring and summer there was greater variability due to nearby wildfires. In winter 2016 and winter 2017, the highest concentrations were associated with quadrant III, where a dense residential area with houses using gas-oil and gas for heating devices is located.

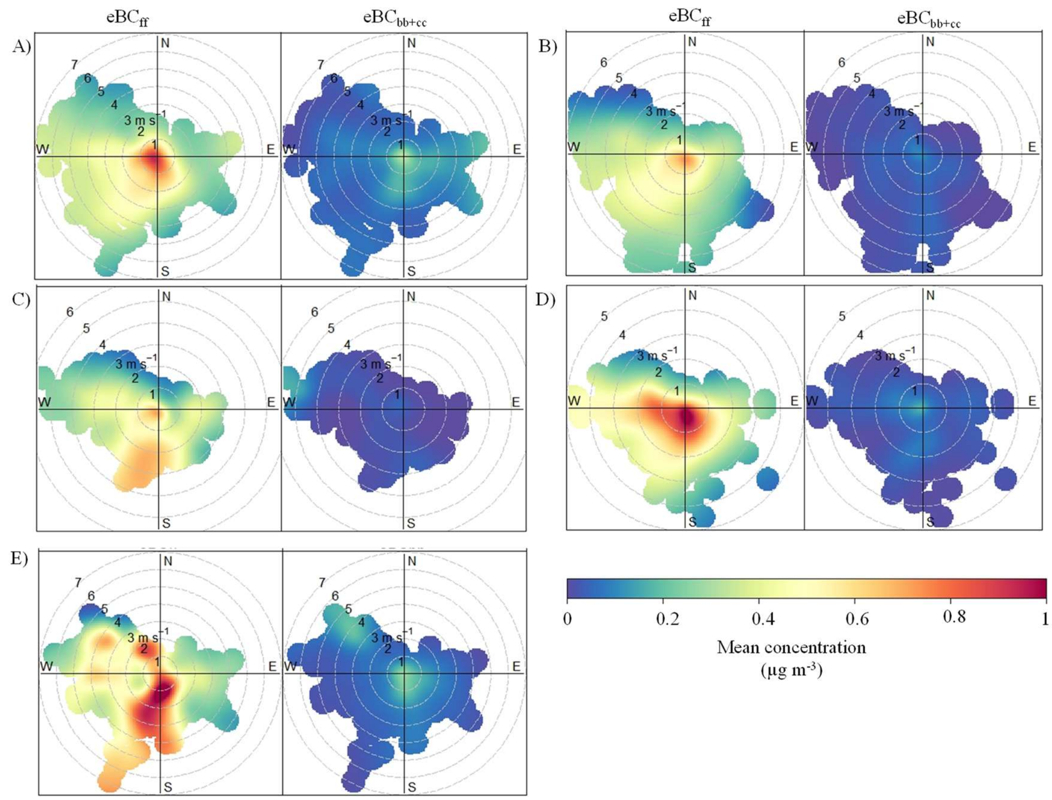

Figure 2. Seasonal polar plot of eBC_{ff} (left) and eBC_{bb+cc} (right) measured at León during the sampling campaign. A) Winter 2016; B) Spring 2016; C) Summer 2016; D) Autumn 2016; E) Winter 2017. The graphs were generated using Openair in R programming (Carslaw, 2015; Carslaw and Ropkins, 2012).

3.1.4. Comparison aethalometer- Thermal optical transmittance methods

PM_{10} concentrations were higher in the cold period than in the warm period (17.0±8.7 vs 12.6±8.3 µg m^{-3}), because of the occurrence of thermal inversions (see ABL in Table A3) and an increase in the use of heating devices in cold months. However, high concentrations were also registered in warm months related to the occurrence of forest fires (Alonso-Blanco et al., 2018b) and Saharan dust intrusions (Díaz et al., 2017).

The daily (24 h samples) eBC/PM_{10} ratio ranged between 0.01 and 0.29, averaging 0.071±0.036 in the cold period and 0.050±0.029 in the warm period. Similar values were obtained in Beijing, also with traffic and coal combustion as important sources of BC during the cold period (Liu et al., 2016b; Yu et al., 2015), whilst lower ratios were registered in Delnice, Croatia, (Godec et al., 2016).

The eBC obtained from the aethalometer and the EC-OC estimated through the thermo-optical method have been correlated. The eBC/OC daily ratio showed higher values in the cold period (0.45±0.17) than in the warm period (0.31±0.13) (Table A6). Similar values were obtained in cities of developing countries such as Dakar and Bamako (Val et al., 2013) and European regions as London, United Kingdom, or Melpitz, Germany (Kendall et al., 2001; Müller, 1999). The ratio estimated for the cold period is typical of fossil fuel and coal combustion (Massling et al., 2015). However, the lower ratio registered during the warm period may be related with biomass burning, which releases ammonia gas and potassium (Yao et al., 2016). The evolution of these ratios along the sampling period is presented in Figure A4.

The EC/eBC daily ratios (Table A5) for the cold period (0.86±0.45) and the warm period (1.09±0.31) are lower than those reported by Liu et al. (2016a) in Tianjin, China, (more differences between EC and eBC were observed in polluted days), but within the range of values compiled by Salako et al. (2012) in nine cities of Asia and Oceania. Thus, the relationship EC-eBC showed a strong positive correlation throughout the sampling period (r=0.84; p<0.01). However, during the cold period, a difference of 8% was observed (Figure 3), mainly on days with EC concentrations higher than 1 $\mu g\ m^{-3}$, similar to what was observed by Liu et al. (2016a). Nevertheless, the fit was better during the cold period (r^2=0.77) than during the warm period (r^2=0.67). Besides, the slope between ligth absorption at 880 nm, assuming the parameters mentioned in paragraph 2.2.1, and EC concentration by the TOT method (Figure A5) has been obtained (4.46±0.16 $m^2\ g^{-1}$). This slope is the mass absorption cross-section (MAC) and it is in the range of values reported by Karanasiou et al. (2015), but it is lower than the values found by Querol et al. (2013) in six Spanish sites, with values ranging between 9.4-15.1 $m^2\ g^{-1}$ in urban and rural sites. It should be remembered that MAC varies as a function of the aerosol composition and age, so it depends on the sampling area and meteorological conditions.

Higher correlations between EC-eBC have been reported in other studies, but many of them are based on a lower number of samples and presented lower concentrations than those of the current research (Ahmed et al., 2009; Hitzenberger et al., 2006; Jeong et al., 2004; Lavanchy et al., 1999; Liu et al., 2016a; Safai et al., 2014). The differences may be due to intersite variability of physical and chemical characteristics of BC, inasmuch as BC particles sometimes are primarily EC but in other cases they are a complex mixture of carbon and non-carbon species (Jeong et al., 2004; Long et al., 2013). Also, filter photometers are cross-sensitive to scattering and overestimate eBC at SSA above 0.85 (Yus-Díez et al., 2021), and anoother factor may be the lensing effect that can increase the eBC/EC ratio (Zhang et al., 2018).

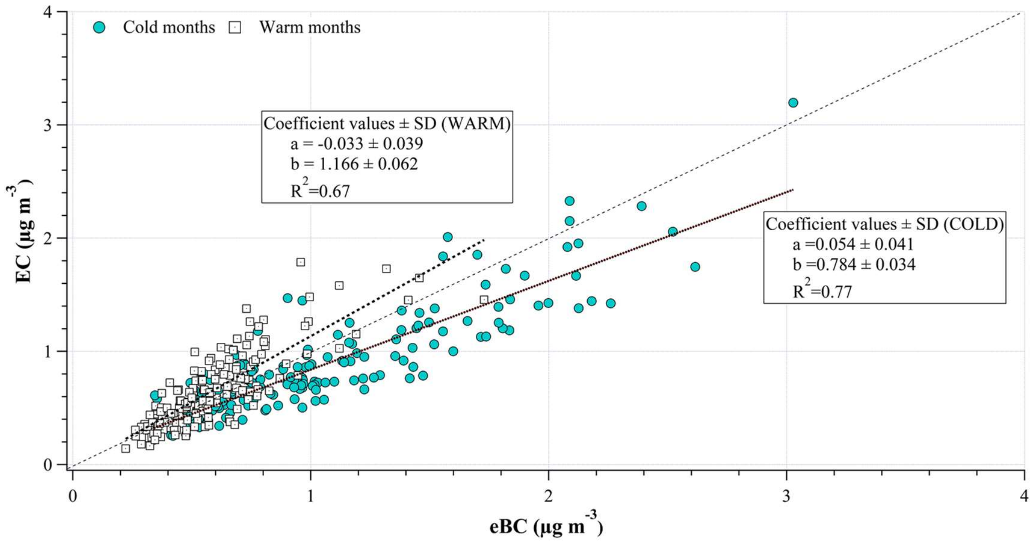

Figure 3. Comparison between EC and eBC throughout the sampling period, discriminating between the cold (circles) and the warm (boxes) period. Dashed line is the 1:1 relation.

3.2. Coal combustion contribution

An analysis of the contribution of coal combustion to the total eBC concentration is shown below assuming the biomass burning fraction, eBC_{bb+cc}, estimated from the aethalometer data after applying the Sandradewi et al. (2008a) approach, and using biomass and coal combustion tracers.

3.2.1. Model variables analysis

Several tracers of biomass burning (levoglucosan, K and Se) and coal combustion (As and SO_2) were evaluated to be used in the construction of the model (Puig et al., 2008; Vejahati et al., 2010; Wang et al., 2018). The tracers with the best fit to the eBC_{bb+cc} data were K (r^2=0.75) and As (r^2=0.56), so they were selected. Other tracers like Se (r^2=0.31), SO_2 (r^2=0.04) or levoglucosan (r^2=0.13) presented a worse fit with eBC_{bb+cc}. For example, the degradation of levoglucosan over time in the atmosphere and/or in the sampling filters (Li et al., 2021) or its emission by other sources like wear between pavement and tyres (Alves et al., 2020) may affect the levoglucosan concentration.

The annual evolution of PM_{10}, As, K and meteorological variables is depicted in Figure 4. The mean concentrations in the cold period were PM_{10} (17.0±8.7 µg m^{-3}), As (0.66±0.86 ng m^{-3}) and K (0.183±0.127 µg m^{-3}), whereas values in the warm period were PM_{10} (12.6±8.3 µg m^{-3}), As (0.11±0.24 ng m^{-3}) and K (0.162±0.126 µg m^{-3}). The mean values for the meteorological variables (T, RH and WS) in the cold period were 7.3±4.1 °C, 69.8±11.4 % and 0.86±0.85 m s^{-1}, while the corresponding values in the warm period were 16.2±5.9 °C, 56.1±12.9 % and 0.97±0.62 m s^{-1}.

The analysis of the remaining variables of the model (eBC_{bb+cc}, percentage of biomass burning and coal combustion (BB+CC(%)) and AAE) was already presented in section 3.1. Although three sources of eBC (eBC_{ff} (traffic), eBC_{bb}, eBC_{cc}) were expected in the cold period, some periods of Saharan dust intrusions were also identified. However, these data were not considered in the present study due to the non-negligible interference that results from the presence of iron oxides associated with this type of events. The contribution of coal combustion to eBC_{bb+cc} for the rest of the year was considered negligible, so in the warm period only two sources were considered (eBC_{ff}, eBC_{bb}).

The variables selected to classify the days - significantly correlated with the independent variable - were temperature, BB+CC (%), AAE, eBC_{bb+cc}, ABL height, As and K concentration.

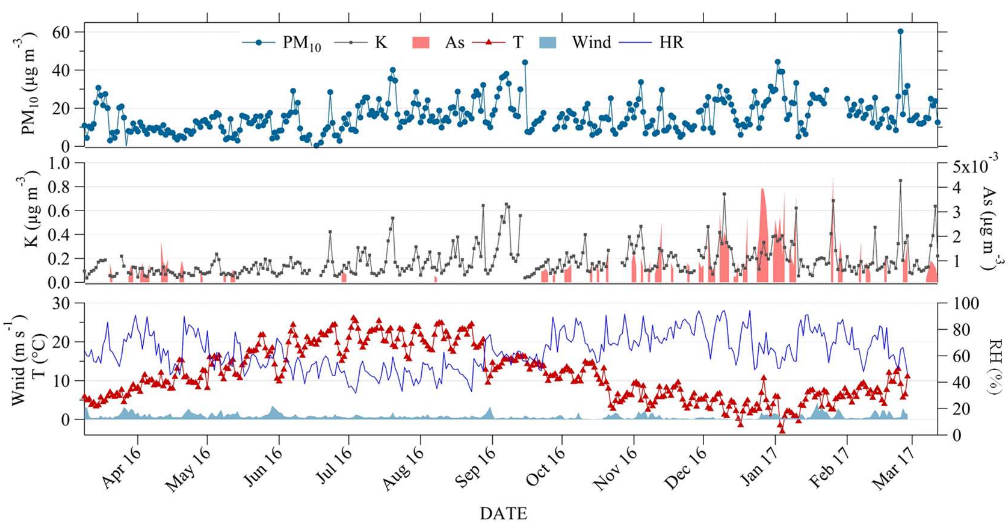

Figure 4. Annual evolution of PM_{10}, As, K and meteorological variables during the sampling campaign.

3.2.2. Model of coal combustion contribution

To select the days to develop the model, two methods have been applied: i) a method based on a two-stage cluster classification was performed for the cold period (from 15 September to 14 April); ii) a method based on As median for the cold period (see Appendix).

From the 7 aforementioned variables (temperature, BB+CC (%), AAE, eBC_{bb+cc}, ABL height, As and K concentration), three clusters were established by grouping the data according to the variables that provided further information (mean values):

- *Cluster 1* corresponds to 49% of the days with an average temperature of 6.1±3.3 °C, an ABL height of 258.1±173.2 m, PM_{10} concentration of 18.1±8.5 µg m^{-3} and:
  - eBC_{bb+cc} concentration of 0.50±0.29 µg m^{-3};
  - K concentration C_K as biomass burning tracer of 0.200±0.105 µg m^{-3};

  - As concentration C_{As} as coal combustion tracer of 1.24±0. 86 ng m^{-3}.
- *Cluster 2* corresponds to 16% of the days with an average temperature of 5.2±3.7 °C, an ABL height of 316.8±259.4 m, PM_{10} concentration of 20.7±9.7 μg m^{-3} and:
  - eBC_{bb+cc} concentration of 0.59±0.31 μg m^{-3};
  - K concentration C_K of 0. 260±0.111 μg m^{-3};
  - As concentration C_{As} of 1.26±0. 61 ng m^{-3}.
- *Cluster 3* includes 35% of the days, with an average temperature of 8.5±3.9 °C, an ABL height of 402.4±192.8 m, PM_{10} concentration of 13.5±6.2 μg m^{-3} and:
  - eBC_{bb+cc} concentration of 0.22±0.11 μg m^{-3};
  - K concentration C_K of 0.149±0.060 μg m^{-3};
  - As concentration C_{As} of 0.75±0.54 ng m^{-3}.

In clusters 1 and 2, the low temperatures and low ABL height could explain the increase in the concentration of biomass burning and coal combustions tracers, while the opposite happens in cluster 3.

Considering that Cluster 3 includes days in which coal combustion emissions could be neglected, the multi-linear regression analysis only considered data from days included in Cluster 1 (N=51) and Cluster 2 (N=16). The estimated eBC_{bb+cc} concentration for biomass burning and coal combustion is expressed as:

$$eBC_{bb+cc}(\mu g\ m^{-3}) = \overbrace{(-0.045 \pm 0.032)}^{\approx zero} + \overbrace{(1.92 \pm 0.15) \times C_K}^{eBC_{bb}} + \overbrace{(119 \pm 20) \times C_{As}}^{eBC_{cc}} \qquad \text{Eq. 1}$$

with a model standard error of 0.11 μg m^{-3}, and a correlation coefficient of *r*=0.92 (Figure 5). Figure A6 shows the time series of eBC_{bb+cc} concentration estimated by the model and eBC_{bb+cc} measured.

The application of this model enabled us to discriminate between eBC_{cc} (mean value of 26% of eBC_{bb+cc}) and eBC_{bb} (mean value of 74% of eBC_{bb+cc}) for the cold period (for days included in clusters 1 and 2). A strong correlation between eBC_{bb} and K (*r*=0.93) and between eBC_{cc} and As (*r*=0.94) has been registered (Figure A7).

In order to prove the goodness of the model, a step-wise automatic linear modelling has been built from a random sample including 75% of the total data set, and this model has then been applied to the remaining 25%. Then, a Kolmogorov-Smirnov statistical test was carried out in order to check the goodness of fit of the model (Table A7). This process has been repeated ten times. The significant values obtained ($\alpha > 0.05$) show that the null hypothesis is confirmed, so measured and predicted data are similar enough. Therefore, the model created from the whole sample may be enforceable. Figure A8 shows a non-cross-correlation between variables included in the model since R^2 between eBC_{cc}-K and eBC_{bb}–As (0.32 and 0.27, respectively) were non-significant. On the other hand, the low values of R^2 between eBC_{bb}-levoglucosan and eBC_{cc}-SO_2 (0.07 and 0.15, respectively) confirm the correct selection of tracers.

The same procedure was repeated, but considering only the days of the cold period with As concentrations higher than the median (0.00082 μg m^{-3}). Similar results were obtained (see Appendix). It should be noted that the main weakness of both models is the daily resolution and future studies will focus on this fact, including variables measured with higher temporal resolution.

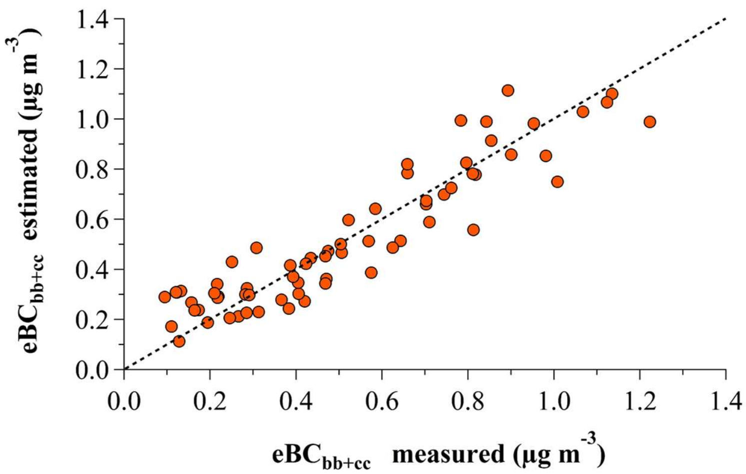

Figure 5. eBC_{bb+cc} concentration estimated by the model vs eBC_{bb+cc} measured. Dashed line is the 1:1 relation.

The mean annual concentrations of eBC_{ff} and eBC_{bb+cc} were 0.58±0.18 and 0.28±0.16 μg m^{-3}, respectively. The model allowed us to estimate mean winter concentrations for eBC_{ff}, eBC_{bb} and eBC_{cc} of 0.65±0.34, 0.27±0.19 and 0.09±0.08 μg m^{-3}, respectively (Table 2). eBC_{bb} concentration was found to be higher in January 2017 (0.49±0.30 μg m^{-3}), more than double the value estimated in January the previous year (0.23±0.11 μg m^{-3}), and four times higher than the concentrations during summer 2016 (0.12±0.11 μg m^{-3}) and spring (0.15±0.07 μg m^{-3}) months. The highest eBC_{cc} levels were estimated for December 2016 and January 2017 (0.18 μg m^{-3}), resulting in the fact that the season with the highest eBC_{cc} concentration was winter 2017 with 0.11±0.10 μg m^{-3}. The low temperatures in winter months promote the use of biomass and coal in heating devices, resulting in the highest levels of eBC_{bb} and eBC_{cc}. The coal combustion percentage CC(%) was almost double in winter (10±2%) when compared to autumn (6±1%), lower percentages than those observed by Liu et al. (2016b) in Beijing, China, an area where the use of coal is more common than in León.

In order to analyse the daily relationship between eBC_{ff}, eBC_{bb}, eBC_{cc} and meteorological parameters (T, RH, WS, VC and ABL height), the daily correlations among these variables have been obtained. Significant ($p<0.05$) negative relationships between T and eBC_{cc} and between T and eBC_{bb} have been found (Table S8), being eBC_{cc} more correlated than eBC_{bb} with T. Also, higher negative correlations have been obtained between eBC_{ff}, eBC_{bb} and eBC_{cc} and WS, VC and ABL height. Besides, non-significant correlations were obtained between RH and eBC from biomass or coal combustion sources. It is important to take into account that eBC_{bb} and eBC_{cc} sources are mainly the same during the cold period (heating devices and coal stoves), so the emission pattern is similar because they are usually used on the same days.

Table 2. Monthly mean values (± standard deviation) calculated for eBC_{ff}, eBC_{bb}, eBC_{cc}, percentage of biomass burning (BB(%)) and coal combustion (CC(%)) from eBC after the application of the model proposed.

Year	Season	Month	eBC_{bb} (µg m^{-3})	eBC_{cc} (µg m^{-3})	BB (%)	CC (%)
2016	Winter	January	0.23±0.11	0.08±0.04	23±7	8±2
	Winter	February	0.20±0.13	0.11±0.07	21±5	11±3
	Spring	March	0.18±0.11	0.08±0.04	25±8	10±3
	Spring	April	0.11±0.04	0.03±0.03	29±7	12±4
	Spring	May	0.13±0.04	-	23±6	-
	Summer	June	0.12±0.11	-	22±8	-
	Summer	July	0.12±0.10	-	22±8	-
	Summer	August	0.12±0.05	-	20±3	-
	Autumn	September	0.21±0.16	0.05±0.03	24±9	6±2
	Autumn	October	0.19±0.08	0.05±0.02	20±5	5±1
	Autumn	November	0.30±0.16	0.08±0.05	27±6	7±2
	Winter	December	0.42±0.20	0.18±0.10	25±6	11±4
2017	Winter	January	0.49±0.30	0.18±0.12	33±11	12±4
	Winter	February	0.25±0.16	0.07±0.04	29±9	9±2
	Spring	March	0.30±0.21	0.06±0.04	36±13	7±2

4. CONCLUSIONS

This paper has studied the temporal evolution of black carbon concentrations in an urban background area located in a coal-mining region, where the use of this fuel is widespread. A model was developed to separate the contribution of BC from biomass burning from the one resulting from coal combustion based on the aethalometer data and tracer concentrations. The annual mean eBC concentration was 0.9±0.9 µg m^{-3}. When correlating eBC with EC, a difference of 12% was observed between the thermo-optical and aethalometer method, especially for eBC concentrations higher than 1 µg m^{-3}.

The combination of coal combustion and biomass burning tracers (As and K, respectively) and the Aethalometer model is shown to be a useful tool for the determination of the three main sources of eBC. For this purpose, the cold days (characterised by a wide use of coal in domestic heating devices) were selected to build a new model.

The Aethalometer model estimates the concentration of biomass burning and traffic based on the assumption that only these two sources are present. In cities where coal remains widely used, the model results should be taken with care, since the smoke from biomass and coal absorbs at the same wavelength. Thus, this study has tried to address a method to differentiate between the concentration from biomass burning (eBC_{bb}) and that from coal combustion (eBC_{cc}) by a multi-linear regression model (r^2=0.85) using the tracers K and As. These contributions in the cold period were, on average, 74% from biomass burning and 26% from coal combustion, resulting in a mean winter concentration for traffic (eBC_{ff}), eBC_{bb} and eBC_{cc} of, respectively, 0.65±0.34, 0.27±0.19 and 0.09±0.08 μg m^{-3}.

The methodology to estimate the contribution of coal combustion to eBC will constitute a useful tool in areas where the use of coal is still widespread. The findings will be crucial in the adoption of mitigation measures to prevent environmental impacts related to coal combustion emissions. Furthermore, the predictive model can be regarded as a first approach to estimate the contribution of coal combustion to black carbon concentrations.

FUNDINGS

This work was partially supported by the AERORAIN project (Ministry of Economy and Competitiveness, Grant CGL2014-52556-R, co-financed with FEDER funds), the University of León (Programa Propio 2018/00203/001), the AEROHEALTH project (Ministry of Science and Innovation, Grant PID2019-106164RB-I00, co-financed with European FEDER funds) and the Junta de Castilla y León (Grant LE025P20, co-financed with European FEDER funds) and the Spanish Ministry of Science, Innovation and Universities (Grant RTI2018-098189-B-I00). This study was also partially supported by SOPRO - Chemical and toxicological SOurce PROfiling of particulate matter in urban air (POCI-01-0145-FEDER-029574), funded by FEDER, through COMPETE2020 - POCI, and by national funds (OE), through FCT/MCTES. We are also grateful for the support to CESAM (UIDB/50017/2020 + UIDP/50017/2020) to FCT/MCTES through national funds, and co-funding by FEDER, within the PT2020 Partnership Agreement and Compete 2020. C. del Blanco Alegre and F. Oduber acknowledge the grants FPU16/05764 and BES-2015-074473 from the Spanish Ministries of Education and of Economy and Competitiveness, respectively. The participation of E. Coz was funded through a CEI Triangular E3 fellowship and MINECO/AEI/FEDER, UE (CGL2017-85344-R). G. Močnik acknowledges support from the Slovenian Research Agency program P1-0385 "Remote sensing of atmospheric properties".

ACKNOWLEDGEMENTS

The authors gratefully acknowledge the NOAA Air Resources Laboratory (ARL) for the provision of the ABL data.

5. REFERENCES

Ahmed, T., Dutkiewicz, V.A., Shareef, A., Tuncel, G., Tuncel, S., Husain, L., 2009. Measurement of black carbon (BC) by an optical method and a thermal-optical method: Intercomparison for four sites. Atmos. Environ. 43, 6305–6311. doi:10.1016/j.atmosenv.2009.09.031

Alonso-Blanco, E., Castro, A., Calvo, A.I., Pont, V., Mallet, M., Fraile, R., 2018a. Wildfire smoke plumes transport under a subsidence inversion: Climate and health implications in a distant urban area. Sci. Total Environ. 619–620, 988–1002. doi:10.1016/j.scitotenv.2017.11.142

Alonso-Blanco, E., Castro, A., Calvo, A.I., Pont, V., Mallet, M., Fraile, R., 2018b. Wildfire smoke plumes transport under a subsidence inversion: Climate and health implications in a distant urban area. Sci. Total Environ. 619–620, 988–1002. doi:10.1016/j.scitotenv.2017.11.142

Alves, C.A., Vicente, A.M.P., Calvo, A.I., Baumgardner, D., Amato, F., Querol, X., Pio, C., Gustafsson, M., 2020. Physical and chemical properties of non-exhaust particles generated from wear between pavements and tyres. Atmos. Environ. 224, 117252. doi:10.1016/j.atmosenv.2019.117252

Andreae, M.O., Gelencsér, A., 2006. Black carbon or brown carbon? the nature of light-absorbing carbonaceous aerosols. Atmos. Chem. Phys. 6, 3131–3148. doi:10.5194/acp-6-3131-2006

Apte, J.S., Marshall, J.D., Cohen, A.J., Brauer, M., 2015. Addressing Global Mortality from Ambient PM2.5. Environ. Sci. Technol. 49, 8057–8066. doi:10.1021/acs.est.5b01236

Auffhammer, M., Ramanathan, V., Vincent, J.R., 2006. Integrated model shows that atmospheric brown clouds and greenhouse gases have reduced rice harvests in India. Proc. Natl. Acad. Sci. 103, 19668–19672. doi:10.1073/pnas.0609584104

Barros, V.R., C.B. Field, D.J. Dokken, M.D. Mastrandrea, K.J. Mach, T.E. Bilir, M. Chatterjee, K.L. Ebi, Y.O. Estrada, R.C. Genova, B. Girma, E.S. Kissel, A.N. Levy, S. MacCracken, P.R.M., (eds.), L.L.W., ICCP, 2014. Climate Change 2014 Impacts, Adaptation, and Vulnerability Part B: Regional Aspects, Igarss 2014. doi:10.1007/s13398-014-0173-7.2

Begam, G.R., Vachaspati, C.V., Ahammed, Y.N., Kumar, K.R., Babu, S.S., Reddy, R.R., 2016. Measurement and analysis of black carbon aerosols over a tropical semi-arid station in Kadapa, India. Atmos. Res. 171, 77–91. doi:10.1016/j.atmosres.2015.12.014

Blanco-Alegre, C., Calvo, A.I., Coz, E., Castro, A., Oduber, F., Prévôt, A.S.H.H., Močnik, G., Fraile, R., 2019. Quantification of source specific black carbon scavenging using an aethalometer and a disdrometer. Environ. Pollut. 246, 336–345.

doi:10.1016/j.envpol.2018.11.102

Blanco-Alegre, C., Calvo, A.I., Fraile, R., 2021. Advances in Environmental Research. Volume 84, in: Daniels, J.A. (Ed.), Advances in Environmental Research. Nova Science Publishers. doi:10.52305/GQSU4556

Bond, T.C., 2001. Spectral dependence of visible light absorption by carbonaceous particles emitted from coal combustion. Geophys. Res. Lett. 28, 4075–4078. doi:10.1029/2001GL013652

Bond, T.C., Covert, D.S., Kramlich, J.C., Larson, T. V, Charlson, R.J., 2002. Primary particle emissions from residential coal burning: Optical properties and size distributions. J. Geophys. Res. Atmos. 107. doi:10.1029/2001JD000571

Bond, T.C., Doherty, S.J., Fahey, D.W., Forster, P.M., Berntsen, T., Deangelo, B.J., Flanner, M.G., Ghan, S., Kürcher, B., Koch, D., Kinne, S., Kondo, Y., Quinn, P.K., Sarofim, M.C., Schultz, M.G., Schulz, M., Venkataraman, C., Zhang, H., Zhang, S., Bellouin, N., Guttikunda, S.K., Hopke, P.K., Jacobson, M.Z., Kaiser, J.W., Klimont, Z., Lohmann, U., Schwarz, J.P., Shindell, D., Storelvmo, T., Warren, S.G., Zender, C.S., 2013. Bounding the role of black carbon in the climate system: A scientific assessment. J. Geophys. Res. Atmos. 118, 5380–5552. doi:10.1002/jgrd.50171

Carslaw, D., 2015. The openair manual open-source tools for analysing air pollution data. King's Coll. London 1, 287.

Carslaw, D.C., Ropkins, K., 2012. Openair - An r package for air quality data analysis. Environ. Model. Softw. 27–28, 52–61. doi:10.1016/j.envsoft.2011.09.008

Casquero-Vera, J.A., Lyamani, H., Titos, G., Minguillón, M.C., Dada, L., Alastuey, A., Querol, X., Petäjä, T., Olmo, F.J., Alados-Arboledas, L., 2021. Quantifying traffic, biomass burning and secondary source contributions to atmospheric particle number concentrations at urban and suburban sites. Sci. Total Environ. 768, 145282. doi:10.1016/j.scitotenv.2021.145282

Castro, L.M., Pio, C.A., Harrison, R.M., Smith, D.J.T., 1999. Carbonaceous aerosol in urban and rural European atmospheres: estimation of secondary organic carbon concentrations. Atmos. Environ. 33, 2771–2781. doi:10.1016/S1352-2310(98)00331-8

Chameides, W., Yu, H., Liu, S., Bergin, M., Xhou, X., Mearns, L., Wang, G., Kiang, C., Saylor, R.D., Luo, C., Huang, Y., Steiner, A., Giorgi, F., 1999. Study of the effects of atmospheric regional haze on agriculture: enhance crop yields in China through emission controls? Proc. Natl. Acad. Sci. 96, 13626–13633.

Chen, X., Kang, S., Yang, J., 2020. Investigation of distribution, transportation, and impact factors of atmospheric black carbon in the Arctic region based on a regional climate-chemistry model. Environ. Pollut. 257, 113127. doi:10.1016/j.envpol.2019.113127

DGT, 2016. Informe anual-Parque vehicular por provincias en España.

Díaz, J., Linares, C., Carmona, R., Russo, A., Ortiz, C., Salvador, P., Machado, R., 2017. Saharan dust intrusions in Spain : Health impacts and associated synoptic conditions. Environ. Res. 156, 455–467. doi:10.1016/j.envres.2017.03.047

Dumka, U.C., Kaskaoutis, D.G., Tiwari, S., Safai, P.D., Attri, S.D., Soni, V.K., Singh, N., Mihalopoulos, N., 2018. Assessment of biomass burning and fossil fuel contribution to black carbon concentrations in Delhi during winter. Atmos. Environ. 194, 93–109. doi:10.1016/j.atmosenv.2018.09.033

EEA, 2016. Air quality in Europe - 2016 Report. Copenhagen, Denmark. doi:10.2800/413142

Fialho, P., Cerqueira, M., Pio, C., Cardoso, J., Nunes, T., Custódio, D., Alves, C., Almeida, S.M., Almeida-Silva, M., Reis, M., Rocha, F., 2014. The application of a multi-wavelength aethalometer to estimate iron dust and black carbon concentrations in the marine boundary layer of Cape Verde. Atmos. Environ. 97, 136–143. doi:10.1016/j.atmosenv.2014.08.008

Fialho, P., Hansen, A.D.A., Honrath, R.E., 2005. Absorption coefficients by aerosols in remote areas: A new approach to decouple dust and black carbon absorption coefficients using seven-wavelength Aethalometer data. J. Aerosol Sci. 36, 267–282. doi:10.1016/j.jaerosci.2004.09.004

Garg, S., Chandra, B.P., Sinha, V., Sarda-Esteve, R., Gros, V., Sinha, B., 2016. Limitation of the use of the absorption angstrom exponent for source apportionment of equivalent black carbon: a case study from the North West Indo-Gangetic plain. Environ. Sci. Technol. 50, 814–824. doi:10.1021/acs.est.5b03868

Godec, R., Jakovljević, I., Šega, K., Čačković, M., Bešlić, I., Davila, S., Pehnec, G., 2016. Carbon species in PM10 particle fraction at different monitoring sites. Environ. Pollut. 216, 700–710. doi:10.1016/j.envpol.2016.06.034

Gonçalves, C., Rienda, I.C., Pina, N., Gama, C., Nunes, T., Tchepel, O., Alves, C., 2021. PM10-Bound Sugars: Chemical Composition, Sources and Seasonal Variations. Atmosphere (Basel). 12, 194. doi:10.3390/atmos12020194

Gramsch, E., Cáceres, D., Oyola, P., Reyes, F., Vásquez, Y., Rubio, M.A., Sánchez, G., 2014. Influence of surface and subsidence thermal inversion on PM2.5 and black carbon concentration. Atmos. Environ. 98, 290–298. doi:10.1016/j.atmosenv.2014.08.066

Hansen, A.D.A., 2005. The Aethalometer, Magee Scientific Corporation. Magee Scientific, Berkeley, CA, USA.

Hansen, A.D.A., Rosen, H., Novakov, T., 1984. The aethalometer - An instrument for the real-time measurement of optical absorption by aerosol particles. Sci. Total Environ. 36, 191–196. doi:10.1016/0048-9697(84)90265-1

Harrison, R.M., Beddows, D.C.S., Jones, A.M., Calvo, A., Alves, C., Pio, C., 2013. An evaluation of some issues regarding the use of aethalometers to measure woodsmoke concentrations.

Atmos. Environ. 80, 540–548. doi:10.1016/j.atmosenv.2013.08.026
Heintzenberg, J., Cereceda-Balic, F., Vidal, V., Leck, C., 2016. Scavenging of black carbon in Chilean coastal fogs. Sci. Total Environ. 541, 341–347. doi:10.1016/j.scitotenv.2015.09.057
Herich, H., Hueglin, C., Buchmann, B., 2011. A 2.5 year's source apportionment study of black carbon from wood burning and fossil fuel combustion at urban and rural sites in Switzerland. Atmos. Meas. Tech. 4, 1409–1420. doi:10.5194/amt-4-1409-2011
Hitzenberger, R., Petzold, A., Bauer, H., Ctyroky, P., Pouresmaeil, P., Laskus, L., Puxbaum, H., 2006. Intercomparison of Thermal and Optical Measurement Methods for Elemental Carbon and Black Carbon at an Urban Location. Environ. Sci. Technol. 40, 6377–6383. doi:10.1021/es051228v
Huang, X., Wang, Z., Ding, A., 2018. Impact of Aerosol-PBL Interaction on Haze Pollution: Multiyear Observational Evidences in North China. Geophys. Res. Lett. 45, 8596–8603. doi:10.1029/2018GL079239
IDAE, 2017. Spanish Institute for Energy Diversification and Saving.
INE, 2017. Cifras oficiales de población resultantes de la revisión del Padrón municipal a 1 de enero de 2016.
Jeong, C.H., Hopke, P.K., Kim, E., Lee, D.W., 2004. The comparison between thermal-optical transmittance elemental carbon and Aethalometer black carbon measured at multiple monitoring sites. Atmos. Environ. 38, 5193–5204. doi:10.1016/j.atmosenv.2004.02.065
Ji, D., Li, L., Pang, B., Xue, P., Wang, L., Wu, Y., Zhang, H., Wang, Y., 2017. Characterization of black carbon in an urban-rural fringe area of Beijing. Environ. Pollut. 223, 1–11. doi:10.1016/j.envpol.2017.01.055
Joshi, H., Naja, M., Singh, K.P., Kumar, R., Bhardwaj, P., Babu, S.S., Satheesh, S.K., Moorthy, K.K., Chandola, H.C., 2016. Investigations of aerosol black carbon from a semi-urban site in the Indo-Gangetic Plain region. Atmos. Environ. 125, 346–359. doi:10.1016/j.atmosenv.2015.04.007
Junta de Castilla y León, 2018. Datos de la Red de Control de la Calidad del Aire. URL: http://servicios.jcyl.es/esco/index.action.
Junta de Castilla y León, 2009. El carbón en Castilla y León. Junta de Castilla y León. Consejería de Economía y Empleo - Dirección General de Energía y Minas.
Junta de Castilla y León, 2008. Encuesta de hogares y medio ambiente. Castilla y León 2008. URL: http://www.jcyl.es/estadistica.
Kang, S., Zhang, Y., Qian, Y., Wang, H., 2020. A review of black carbon in snow and ice and its impact on the cryosphere. Earth-Science Rev. 210, 103346. doi:10.1016/j.earscirev.2020.103346
Karanasiou, A., Minguillón, M. C., Viana, M., Alastuey, A., Putaud, J.-P., Maenhaut, W.,

Panteliadis, P., Močnik, G., Favez, O., and Kuhlbusch, T.A.J., 2015. Thermal-optical analysis for the measurement of elemental carbon (EC) and organic carbon (OC) in ambient air a literature review. Atmos. Meas. Tech. 8, 9649–9712. doi:10.5194/amtd-8-9649-2015

Kendall, M., Hamilton, R.S., Watt, J., Williams, I.D., 2001. Characterisation of selected speciated organic compounds associated with particulate matter in London. Atmos. Environ. 35, 2483–2495. doi:10.1016/S1352-2310(00)00431-3

Kinney, P.L., 2008. Climate change, air quality, and human health. Am. J. Prev. Med. 35, 459–467. doi:10.1016/j.amepre.2008.08.025

Kirchstetter, T.W., Novakov, T., Hobbs, P. V., 2004. Evidence that the spectral dependence of light absorption by aerosols is affected by organic carbon. J. Geophys. Res. D Atmos. 109, 1–12. doi:10.1029/2004JD004999

Klompmaker, J.O., Montagne, D.R., Meliefste, K., Hoek, G., Brunekreef, B., 2015. Spatial variation of ultrafine particles and black carbon in two cities: Results from a short-term measurement campaign. Sci. Total Environ. 508, 266–275. doi:10.1016/j.scitotenv.2014.11.088

Kucbel, M., Corsaro, A., Švédová, B., Raclavská, H., Raclavský, K., Juchelková, D., 2017. Temporal and seasonal variations of black carbon in a highly polluted European city: Apportionment of potential sources and the effect of meteorological conditions. J. Environ. Manage. 203, 1178–1189. doi:10.1016/j.jenvman.2017.05.038

Kuhlbusch, T., Borowiak, A., Gelencser, A., Genberg, J., Gladtke, D., Maenhaut, W., Pio, C., Popoviecheva, O., Putaud, J.-P., Quincey, P., Sciare, J., ten Brink, H., Viana, M., Yttri, K., 2009. Measurement of elemental and organic carbon in Europe, JRC Scientific and Technical Reports. doi:10.2788/34791

Lavanchy, V.M.H., Gäggeler, H.W., Nyeki, S., Baltensperger, U., 1999. Elemental carbon (EC) and black carbon (BC) measurements with a thermal method and an aethalometer at the high-alpine research station Jungfraujoch. Atmos. Environ. 33, 2759–2769. doi:10.1016/S1352-2310(98)00328-8

Lelieveld, J., Evans, J.S., Fnais, M., Giannadaki, D., Pozzer, A., 2015. The contribution of outdoor air pollution sources to premature mortality on a global scale. Nature 525, 367–371. doi:10.1038/nature15371

Li, Y., Fu, T.M., Yu, J.Z., Feng, X., Zhang, L., Chen, J., Boreddy, S.K.R., Kawamura, K., Fu, P., Yang, X., Zhu, L., Zeng, Z., 2021. Impacts of Chemical Degradation on the Global Budget of Atmospheric Levoglucosan and Its Use As a Biomass Burning Tracer. Environ. Sci. Technol. 55, 5525–5536. doi:10.1021/acs.est.0c07313

Liakakou, E., Stavroulas, I., Kaskaoutis, D.G., Grivas, G., Paraskevopoulou, D., Dumka, U.C., Tsagkaraki, M., Bougiatioti, A., Oikonomou, K., Sciare, J., Gerasopoulos, E., Mihalopoulos, N., 2020. Long-term variability, source apportionment and spectral properties of black carbon at an urban background site in Athens, Greece. Atmos. Environ. 222, 117137. doi:10.1016/j.atmosenv.2019.117137

Liu, B., Bi, X., Feng, Y., Dai, Q., Xiao, Z., Li, L., Wu, J., 2016. Fine carbonaceous aerosol characteristics at a megacity during the Chinese Spring Festival as given by OC / EC online measurements. Atmos. Res. 181, 20–28. doi:10.1016/j.atmosres.2016.06.007

Liu, Q., Ma, T., Olson, M.R., Liu, Y., Zhang, T., Wu, Y., Schauer, J.J., 2016. Temporal variations of black carbon during haze and non-haze days in Beijing. Sci. Rep. 6, 1–10. doi:10.1038/srep33331

Long, C.M., Nascarella, M.A., Valberg, P.A., 2013. Carbon black vs. black carbon and other airborne materials containing elemental carbon: Physical and chemical distinctions. Environ. Pollut. 181, 271–286. doi:10.1016/j.envpol.2013.06.009

Lucarelli, F., Calzolai, G., Chiari, M., Giannoni, M., Mochi, D., Nava, S., Carraresi, L., 2014. The upgraded external-beam PIXE/PIGE set-up at LABEC for very fast measurements on aerosol samples. Nucl. Instruments Methods Phys. Res. Sect. B Beam Interact. with Mater. Atoms 318, 55–59. doi:10.1016/j.nimb.2013.05.099

Lucas-Borja, M.E., Madrigal, J., Candel-Pérez, D., Jiménez, E., Moya, D., Heras, J. de las, Guijarro, M., Vega, J.A., Fernández, C., Hernando, C., 2016. Effects of prescribed burning, vegetation treatment and seed predation on natural regeneration of Spanish black pine (Pinus nigra Arn. ssp. salzmannii) in pure and mixed forest stands. For. Ecol. Manage. 378, 24–30. doi:10.1016/j.foreco.2016.07.019

Lyamani, H., Fernández-Gálvez, J., Pérez-Ramírez, D., Valenzuela, A., Antón, M., Alados, I., Titos, G., Olmo, F.J., Alados-Arboledas, L., 2012. Aerosol properties over two urban sites in South Spain during an extended stagnation episode in winter season. Atmos. Environ. 62, 424–432. doi:10.1016/j.atmosenv.2012.08.050

Marín, J.C., Raga, G.B., Arévalo, J., Baumgardner, D., Córdova, A.M., Pozo, D., Calvo, A., Castro, A., Fraile, R., Sorribas, M., 2017. Properties of particulate pollution in the port city of Valparaiso, Chile. Atmos. Environ. 171, 301–316. doi:10.1016/j.atmosenv.2017.09.044

Massling, A., Nielsen, I.E., Kristensen, D., Christensen, J.H., Sorensen, L.L., Jensen, B., Nguyen, Q.T., Nøjgaard, J.K., Glasius, M., Skov, H., 2015. Atmospheric black carbon and sulfate concentrations in Northeast Greenland. Atmos. Chem. Phys. 15, 9681–9692. doi:10.5194/acp-15-9681-2015

Meena, G.S., Mukherjee, S., Buchunde, P., Safai, P.D., Singla, V., Aslam, M.Y., Sonbawne, S.M., Made, R., Anand, V., Dani, K.K., Pandithurai, G., 2021. Seasonal variability and source apportionment of black carbon over a rural high-altitude and an urban site in western India. Atmos. Pollut. Res. 12, 32–45. doi:10.1016/j.apr.2020.10.006

Moreira, G. de A., Guerrero-Rascado, J.L., Bravo-Aranda, J.A., Foyo-Moreno, I., Cazorla, A., Alados, I., Lyamani, H., Landulfo, E., Alados-Arboledas, L., 2020. Study of the planetary boundary layer height in an urban environment using a combination of microwave radiometer and ceilometer. Atmos. Res. 240, 104932. doi:10.1016/j.atmosres.2020.104932

Müller, K., 1999. A 3 year study of the aerosol in northwest Saxony (Germany). Atmos. Environ. 33, 1679–1685. doi:10.1016/S1352-2310(98)00333-1

NOAA, 2017. National Oceanic and Atmospheric Administration.

Oduber, F., Calvo, A.I., Blanco-Alegre, C., Castro, A., Vega-Maray, A.M., Valencia-Barrera, R.M., Fernández-González, D., Fraile, R., 2019. Links between recent trends in airborne pollen concentration, meteorological parameters and air pollutants. Agric. For. Meteorol. 264, 16–26. doi:10.1016/j.agrformet.2018.09.023

Oduber, F., Calvo, A.I., Castro, A., Blanco-Alegre, C., Alves, C., Calzolai, G., Nava, S., Lucarelli, F., Nunes, T., Barata, J., Fraile, R., 2021. Characterization of aerosol sources in León (Spain) using Positive Matrix Factorization and weather types. Sci. Total Environ. 754, 142045. doi:10.1016/j.scitotenv.2020.142045

Pachon, J.E., Weber, R.J., Zhang, X., Mulholland, J.A., Russell, A.G., 2013. Revising the use of potassium (K) in the source apportionment of PM2.5. Atmos. Pollut. Res. 4, 14–21. doi:10.5094/APR.2013.002

Petzold, A., Ogren, J.A., Fiebig, M., Laj, P., Li, S.M., Baltensperger, U., Holzer-Popp, T., Kinne, S., Pappalardo, G., Sugimoto, N., Wehrli, C., Wiedensohler, A., Zhang, X.Y., 2013. Recommendations for reporting black carbon measurements. Atmos. Chem. Phys. 13, 8365–8379. doi:10.5194/acp-13-8365-2013

Pio, C., Cerqueira, M., Harrison, R.M., Nunes, T., Mirante, F., Alves, C., Oliveira, C., Sanchez, A., Campa, D., Artíñano, B., Matos, M., 2011. OC / EC ratio observations in Europe : Re-thinking the approach for apportionment between primary and secondary organic carbon. Atmos. Environ. 45, 6121–6132. doi:10.1016/j.atmosenv.2011.08.045

Pokhrel, R.P., Wagner, N.L., Langridge, J.M., Lack, D.A., Jayarathne, T., Stone, E.A., Stockwell, C.E., Yokelson, R.J., Murphy, S.M., 2016. Parameterization of single-scattering albedo (SSA) and absorption Ångström exponent (AAE) with EC/OC for aerosol emissions from biomass burning. Atmos. Chem. Phys. 16, 9549–9561. doi:10.5194/acp-16-9549-2016

Puig, R., Àvila, A., Soler, A., 2008. Sulphur isotopes as tracers of the influence of a coal-fired power plant on a Scots pine forest in Catalonia (NE Spain). Atmos. Environ. 42, 733–745. doi:10.1016/j.atmosenv.2007.09.059

Querol, X., Alastuey, A., Viana, M., Moreno, T., Reche, C., Minguillón, M.C., Ripoll, A., Pandolfi, M., Amato, F., Karanasiou, A., Pérez, N., Pey, J., Cusack, M., Vázquez, R., Plana, F., Dall'Osto, M., De La Rosa, J., Sánchez De La Campa, A., Fernández-Camacho, R., Rodríguez, S., Pio, C., Alados-Arboledas, L., Titos, G., Artíñano, B., Salvador, P., García Dos Santos, S., Fernández Patier, R., 2013. Variability of carbonaceous aerosols in remote, rural, urban and industrial environments in Spain: Implications for air quality policy. Atmos. Chem. Phys. 13, 6185–6206. doi:10.5194/acp-13-6185-2013

Reche, C., Querol, X., Alastuey, A., Viana, M., Pey, J., Moreno, T., Rodríguez, S., González, Y., Fernández-Camacho, R., De La Campa, A.M.S., De La Rosa, J., Dall'Osto, M., Prévt, A.S.H., Hueglin, C., Harrison, R.M., Quincey, P., 2011. New considerations for PM, Black Carbon and particle number concentration for air quality monitoring across different European cities. Atmos. Chem. Phys. 11, 6207–6227. doi:10.5194/acp-11-6207-2011

Russell, P.B., Bergstrom, R.W., Shinozuka, Y., Clarke, D., DeCarlo, P.F., Jimenez, J.L., Livingston, J.M., Redemann, J., Holben, B., Dubovik, O., Strawa, A., 2009. Absorption Angstrom Exponent in AERONET and related data as an indicator of aerosol composition. Atmos. Chem. Phys. Discuss. 9, 21785–21817. doi:10.5194/acpd-9-21785-2009

Saenen, N.D., Provost, E.B., Viaene, M.K., Vanpoucke, C., Lefebvre, W., Vrijens, K., Roels, H.A., Nawrot, T.S., 2016. Recent versus chronic exposure to particulate matter air pollution in association with neurobehavioral performance in a panel study of primary schoolchildren. Environ. Int. 95, 112–119. doi:10.1016/j.envint.2016.07.014

Safai, P.D., Raju, M.P., Rao, P.S.P., Pandithurai, G., 2014. Characterization of carbonaceous aerosols over the urban tropical location and a new approach to evaluate their climatic importance. Atmos. Environ. 92, 493–500. doi:10.1016/j.atmosenv.2014.04.055

Salako, G.O., Hopke, P.K., Cohen, D.D., Begum, B.A., Biswas, S.K., Pandit, G.G., Chung, Y.S., Rahman, S.A., Hamzah, M.S., Davy, P., Markwitz, A., Shagjjamba, D., Lodoysamba, S., Wimolwattanapun, W., Bunprapob, S., 2012. Exploring the variation between EC and BC in a variety of locations. Aerosol Air Qual. Res. 12, 1–7. doi:10.4209/aaqr.2011.09.0150

Sandradewi, J., Prévôt, A.S.H., Szidat, S., Perron, N., Alfarra, M.R., Lanz, V.A., Weingartner, E., Baltensperger, U.R.S., 2008a. Using aerosol light absorption measurements for the quantitative determination of wood burning and traffic emission contribution to particulate matter. Environ. Sci. Technol. 42, 3316–3323. doi:10.1021/es702253m

Sandradewi, J., Prévôt, A.S.H., Weingartner, E., Schmidhauser, R., Gysel, M., Baltensperger, U., 2008b. A study of wood burning and traffic aerosols in an Alpine valley using a multi-wavelength Aethalometer. Atmos. Environ. 42, 101–112. doi:10.1016/j.atmosenv.2007.09.034

Shen, L., Wang, H., Kong, X., Yin, Y., Chen, K., Chen, J., 2021. Characterization of black carbon aerosol at the summit of Mount Tai (1534 m) in central east China: Temporal variation, source appointment and transport. Atmos. Environ. 246, 118152. doi:10.1016/j.atmosenv.2020.118152

Spanish Ministry for the Ecological Transition, 2018. Spanish Ministry for the Ecological Transition.

Sun, J., Zhi, G., Hitzenberger, R., Chen, Y., Tian, C., Zhang, Yayun, Feng, Y., Cheng, M., Zhang, Yuzhe, Cai, J., Chen, F., Qiu, Y., Jiang, Z., Li, J., Zhang, G., Mo, Y., 2017. Emission factors and light absorption properties of brown carbon from household coal combustion in China. Atmos. Chem. Phys. 17, 4769–4780. doi:10.5194/acp-17-4769-2017

Tan, Y., Wang, H., Shi, S., Shen, L., Zhang, C., Zhu, B., Guo, S., Wu, Z., Song, Z., Yin, Y., Liu, A., 2020. Annual variations of black carbon over the Yangtze River Delta from 2015 to 2018. J. Environ. Sci. (China) 96, 72–84. doi:10.1016/j.jes.2020.04.019

Tang, G., Zhao, P., Wang, Yinghong, Gao, W., Cheng, M., Xin, J., Li, X., Wang, Yuesi, 2017. Mortality and air pollution in Beijing: The long-term relationship. Atmos. Environ. 150, 238–243. doi:10.1016/j.atmosenv.2016.11.045

Tobler, A., Bhattu, D., Canonaco, F., Lalchandani, V., Shukla, A., Thamban, N.M., Mishra, S., Srivastava, A.K., Bisht, D.S., Tiwari, S., Singh, S., Močnik, G., Baltensperger, U., Tripathi, S.N., Slowik, J.G., Prévôt, A.S.H., 2020. Chemical characterization of PM2.5 and source apportionment of organic aerosol in New Delhi, India. Sci. Total Environ. 745, 1–12. doi:10.1016/j.scitotenv.2020.140924

Tong, Z., Chen, Y., Malkawi, A., Adamkiewicz, G., Spengler, J.D., 2016. Quantifying the impact of traffic-related air pollution on the indoor air quality of a naturally ventilated building. Environ. Int. 89–90, 138–146. doi:10.1016/j.envint.2016.01.016

Tong, Z., Yang, B., Hopke, P.K., Zhang, K.M., 2017. Microenvironmental air quality impact of a commercial-scale biomass heating system. Environ. Pollut. 220, 1112–1120. doi:10.1016/j.envpol.2016.11.025

Val, S., Liousse, C., Doumbia, E.H.T., Galy-Lacaux, C., Cachier, H., Marchand, N., Badel, A., Gardrat, E., Sylvestre, A., Baeza-Squiban, A., 2013. Physico-chemical characterization of African urban aerosols (Bamako in Mali and Dakar in Senegal) and their toxic effects in human bronchial epithelial cells: Description of a worrying situation. Part. Fibre Toxicol. 10. doi:10.1186/1743-8977-10-10

Vejahati, F., Xu, Z., Gupta, R., 2010. Trace elements in coal: Associations with coal and minerals and their behavior during coal utilization - A review. Fuel 89, 904–911. doi:10.1016/j.fuel.2009.06.013

Wang, C., Liu, H., Zhang, Y., Zou, C., Anthony, E.J., 2018. Review of arsenic behavior during coal combustion : Volatilization , transformation , emission and removal technologies. Prog. Energy Combust. Sci. 68, 1–28. doi:10.1016/j.pecs.2018.04.001

Weichenthal, S., Farrell, W., Goldberg, M., Joseph, L., Hatzopoulou, M., 2014. Characterizing the impact of traffic and the built environment on near-road ultrafine particle and black carbon concentrations. Environ. Res. 132, 305–310. doi:10.1016/j.envres.2014.04.007

Weingartner, E., Saathoff, H., Schnaiter, M., Streit, N., Bitnar, B., Baltensperger, U., 2003. Absorption of light by soot particles: Determination of the absorption coefficient by means of aethalometers. J. Aerosol Sci. 34, 1445–1463. doi:10.1016/S0021-8502(03)00359-8

WHO/United Nations, 2018. Residential heating with wood and coal: health impacts and policy options in Europe and North America.

WHO, 2013. Review of evidence on health aspects of air pollution – REVIHAAP Project, World Health Organization. Copenhagen, Denmark.

WHO, 2012. Health effects of Black carbon. Copenhagen, Denmark.

WMO, 2016. WMO/GAW Aerosol Measurement procedures guidelines and recommendations, GAW Report. Geneva, Switzerland.

Wu, M., Liu, X., Zhang, L., Wu, C., Lu, Z., Ma, P.L., Wang, H., Tilmes, S., Mahowald, N., Matsui, H., Easter, R.C., 2018. Impacts of Aerosol Dry Deposition on Black Carbon Spatial Distributions and Radiative Effects in the Community Atmosphere Model CAM5. J. Adv. Model. Earth Syst. 10, 1150–1171. doi:10.1029/2017MS001219

Xie, M., Shen, G., Holder, A.L., Hays, M.D., Jetter, J.J., 2018. Light absorption of organic carbon emitted from burning wood, charcoal, and kerosene in household cookstoves. Environ. Pollut. 240, 60–67. doi:10.1016/j.envpol.2018.04.085

Yang, Y., Fu, Y., Lin, Q., Jiang, F., Lian, X., Li, L., Wang, Z., Zhang, G., Bi, X., Wang, X., Sheng, G., 2019. Recent advances in quantifying wet scavenging efficiency of black carbon aerosol. Atmosphere (Basel). 10, 1–19. doi:10.3390/atmos10040175

Yao, L., Yang, L., Chen, J., Wang, X., Xue, L., Li, W., Sui, X., Wen, L., Chi, J., Zhu, Y., Zhang, J., Xu, C., Zhu, T., Wang, W., 2016. Characteristics of carbonaceous aerosols: Impact of biomass burning and secondary formation in summertime in a rural area of the North China Plain. Sci. Total Environ. 557–558, 520–530. doi:10.1016/j.scitotenv.2016.03.111

Yu, N., Zhu, Y., Xie, X., Yan, C., Zhu, T., Zheng, M., 2015. Characterization of ultrafine particles and other traffic related pollutants near roadways in Beijing. Aerosol Air Qual. Res. 15, 1261–1269. doi:10.4209/aaqr.2014.11.0295

Yus-Díez, J., Bernardoni, V., Močnik, G., Alastuey, A., Ciniglia, D., Ivančič, M., Querol, X., Perez, N., Reche, C., Rigler, M., Vecchi, R., Valentini, S., Pandolfi, M., 2021. Determination of the multiple-scattering correction factor and its cross-sensitivity to scattering and wavelength dependence for different AE33 Aethalometer filter tapes: A multi-instrumental approach. Atmos. Meas. Tech. Discuss. 2021, 1–30.

Zhang, Y., Favez, O., Canonaco, F., Liu, D., Močnik, G., Amodeo, T., Sciare, J., Prévôt, A.S.H., Gros, V., Albinet, A., 2018. Evidence of major secondary organic aerosol contribution to lensing effect black carbon absorption enhancement. npj Clim. Atmos. Sci. 1, 47.

doi:10.1038/s41612-018-0056-2

Zhu, X., Tang, G., Lv, F., Hu, B., Cheng, M., Münkel, C., Schäfer, K., Xin, J., An, X., Wang, G., Li, X., Wang, Y., 2018. The spatial representativeness of mixing layer height observations in the North China Plain. Atmos. Res. 209, 204–211. doi:10.1016/j.atmosres.2018.03.019

Zotter, P., Herich, H., Gysel, M., El-Haddad, I., Zhang, Y., Močnik, G., Hüglin, C., Baltensperger, U., Szidat, S., Prévôt, A.S.H., 2017. Evaluation of the absorption Ångström exponents for traffic and wood burning in the Aethalometer based source apportionment using radiocarbon measurements of ambient aerosol. Atmos. Chem. Phys. 17, 4229–4249. doi:10.5194/acp-17-4229-2017

Contribution of coal combustion to black carbon: coupling tracers with the aethalometer model

C. Blanco-Alegre[1], P. Fialho[2], A.I. Calvo[1], A. Castro[1], E. Coz[3], F. Oduber[1], A.S.H. Prévôt[4], G. Močnik[5,6], C. Alves[7], F. Giardi[8], G. Pazzi[8], R. Fraile[1]

[1]Department of Physics, IMARENAB University of León, 24071 León, Spain

[2]Institute of Volcanology and Risk Assessment – IVAR, Rua da Mãe de Deus, 9500-321 Ponta Delgada, Portugal

[3]Centre for Energy, Environment and Technology Research (CIEMAT), Department of the Environment, Madrid, Spain

[4]Laboratory of Atmospheric Chemistry, Paul Scherrer Institute, 5232 Villigen, Switzerland

[5]Center for Atmospheric Research, University of Nova Gorica, 5270 Ajdovščina, Slovenia

[6]Condensed Matter Physics Dept., Jožef Stefan Institute, 1000 Ljubljana, Slovenia

[7]Centre for Environmental and Marine Studies (CESAM), Department of Environment and Planning, University of Aveiro, Aveiro 3810-193, Portugal

[8]Department of Physics and Astronomy, Università di Firenze and INFN-Firenze, 50019 Sesto Fiorentino, Italy

Corresponding Author: aicalg@unileon.es *+34987291543*

1. APPENDIX

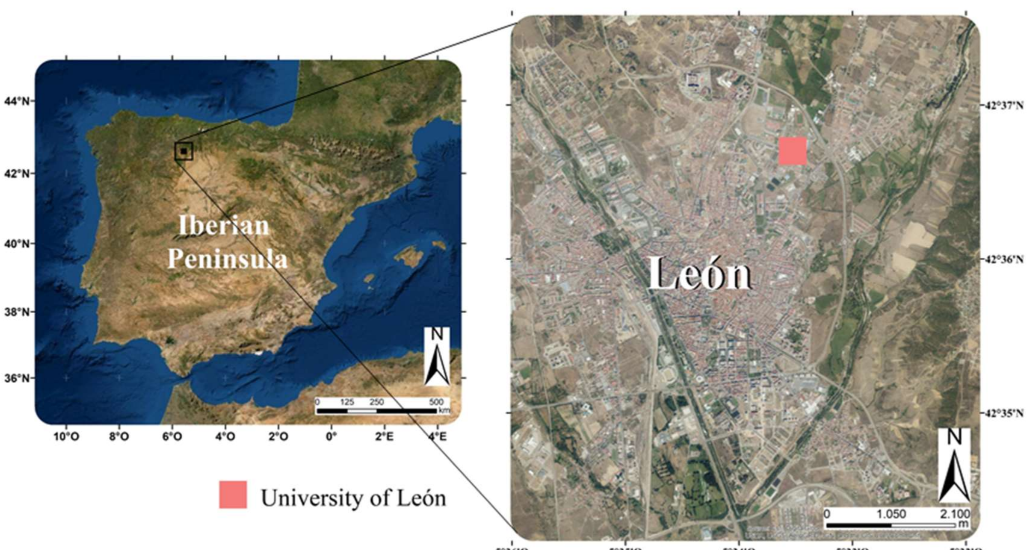

Figure A1. Geographic location of the city of León, Spain (left) and sampling site. Source: Earthstar Geographics, ESRI.

a)

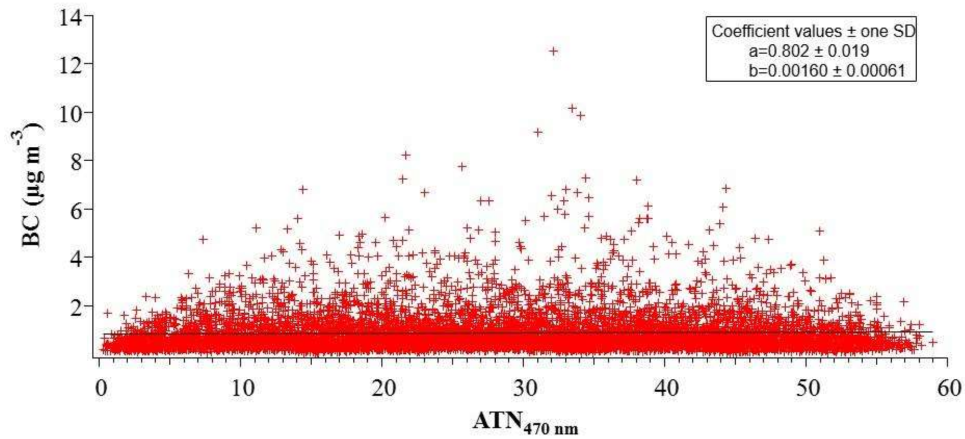
Coefficient values ± one SD
a=0.802 ± 0.019
b=0.00160 ± 0.00061
BC (µg m-3)
ATN470 nm

b)

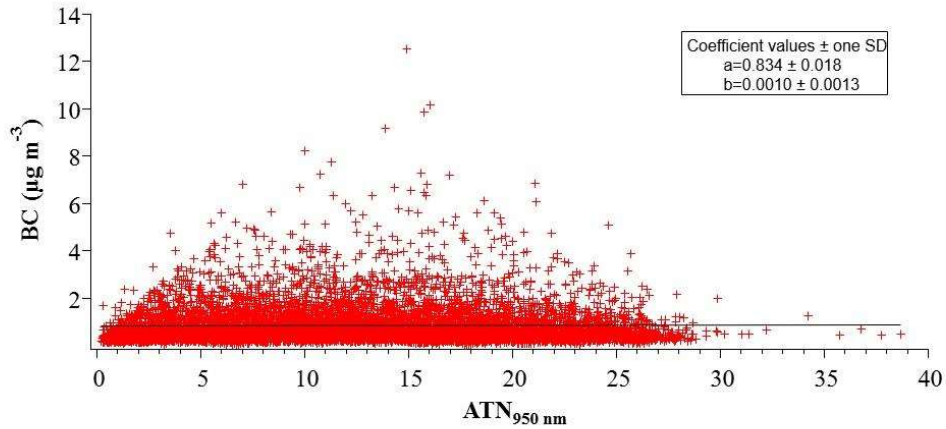
Coefficient values ± one SD
a=0.834 ± 0.018
b=0.0010 ± 0.0013
BC (µg m-3)
ATN950 nm

c)

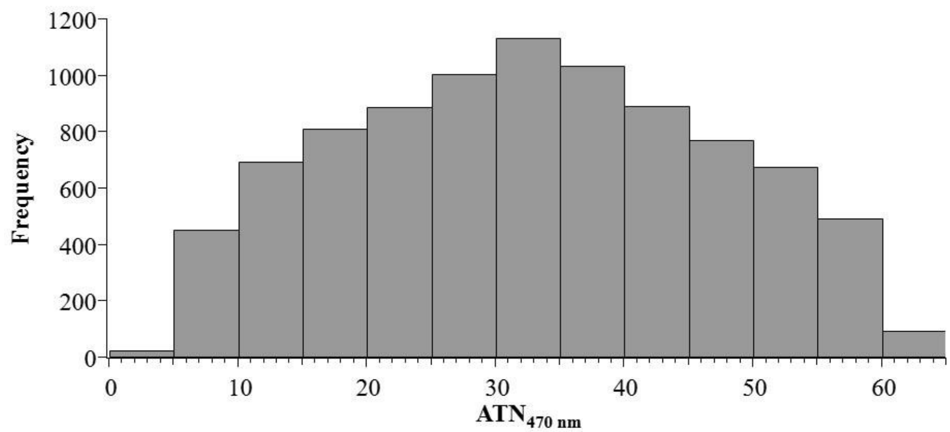
Frequency
ATN470 nm

d)

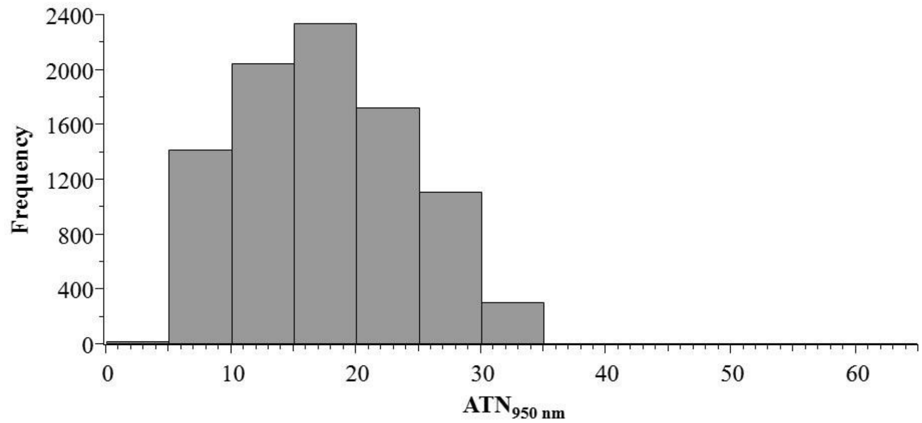

e)

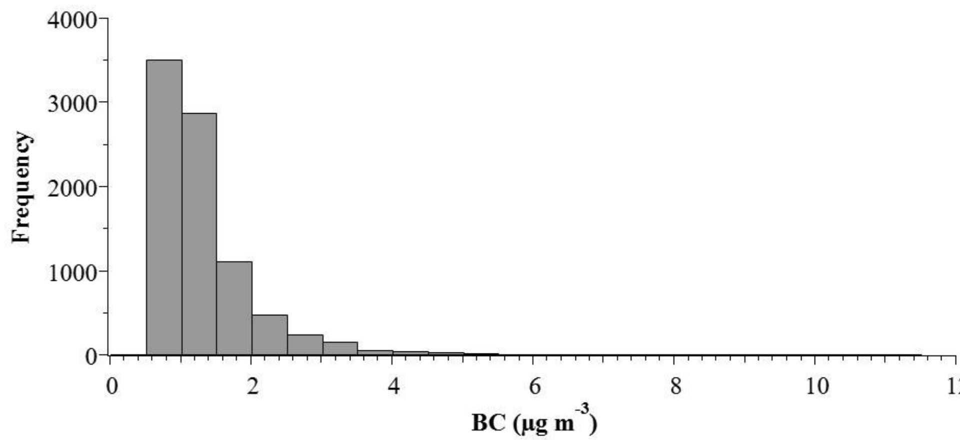

Figure A2. BC as a function of a) $ATN_{470\ nm}$ and b) $ATN_{950\ nm}$ plot; c) Frequency distribution of the number of measurements per $ATN_{470\ nm}$; d) Frequency distribution of the number of measurements per $ATN_{950\ nm}$; e) The BC frequency in the ATN range of 10-75.

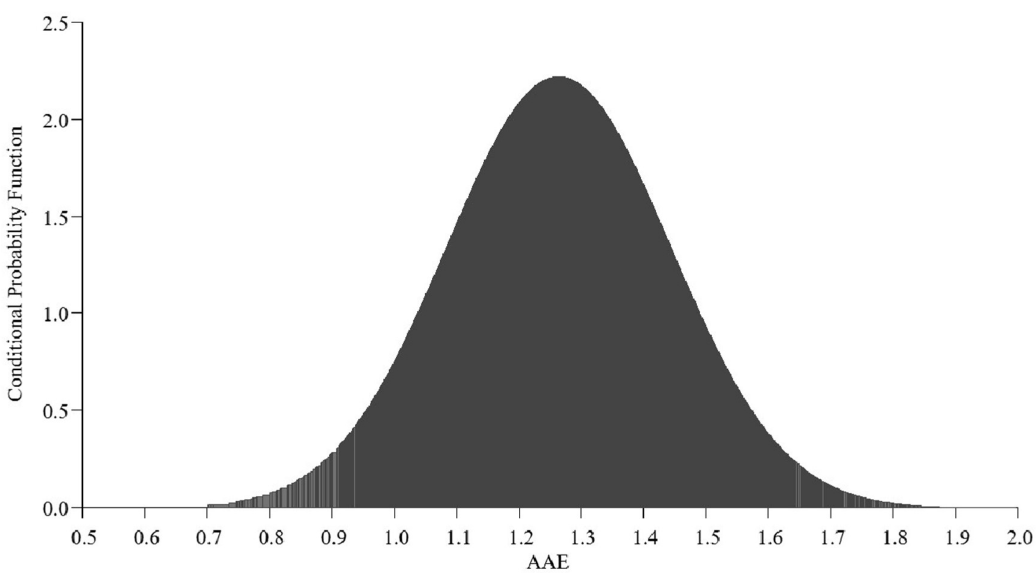

Figure A3. Probability distribution function of the AAE (470/950) over the full campaign.

Table A1. Parameters $f(\lambda_w)$ or the compensation of the "load effect" of each αw as a function of the cold or warm period of the year.

α_w (nm)	370	470	520	590	660	880	950
$f(\alpha_w)$ Cold period	1.155	1.137	1.128	1.116	1.103	1.064	1.051
$f(\alpha_w)$ Warm period	1.141	1.132	1.127	1.120	1.114	1.093	1.086

Table A2. Comparison of eBC concentrations (μg m^{-3}) measured in this study and values reported in the literature.

Station	Location	Environment type	Period	eBC (μg m^{-3})	Reference
León (Spain)	42°36′N, 05°35′W, 838 m	Urban background	Jan.2016-Mar. 2017	0.9±0.9	Present study
Valparaiso (Chile)	33º01′S, 71º37′W, 80 m	Urban	Dec.2014-Jan. 2015	0.8-0.9	(Marín et al., 2017)
Pantnagar (India)	29°00′N, 79°30′W, 231 m	Urban background	2009-2012	5.5±4.7	(Joshi et al., 2016)
Rome (Italy)	44°25'N,12°12'E, 20 m	Urban background	May-Jun. 2012	1.7±1.2	(Costabile et al., 2015)
Beijing (China)	40°03′N, 116°25′E, 535 m	Urban-rural fringe	2014	4.4±3.7	(Ji et al., 2017)
New York (USA)	40°48'N, 73°54"W, 20 m	Urban	2003-2011	1.4-2	(Rattigan et al., 2013)
Ostrava (Czech Republic)	49°47′N, 18°13′E, 230 m	Urban	2012-2014	3.5±4.1	(Kucbel et al., 2017)
London (UK)	51°30′N, 0°07′E, 25m	Urban	Jan.-Aug. 2012	1.3±1.1	(Liu et al., 2014)
Amsterdam (Netherlands)	52°23′N, 4°54′E, 0 m	Urban background	Jan.-Jul.2013	0.8±0.5	(Klompmaker et al., 2015)
Rotterdam (Netherlands)	51°55′N 4°28′E, 0 m	Urban background		1.4± 0.6	
Montreal (Canada)	45°30′N, 73°35′O, 216 m	Urban	Jun.- Jul. 2012	1.1±1.3	(Weichenthal et al., 2014)
Athens (Greece)	37º58'N, 23º43', 105 m	Urban background	May 2015–Apr. 2019	1.9±2.5	(Liakakou et al., 2020)
Granada (Spain)	7.18°N, 3.58°W, 680 m	Suburban Urban	Dec. 2015- Apr.2016 Dec. 2015- Apr.2016	2.9±3.0 3.0±3.0	(Casquero-Vera et al., 2021)
Santa Cruz Tenerife (Spain)	28º29'N, 16º18'W, 52 m	Urban background	Jan.-Dec. 2009	0.8±0.4	(Reche et al., 2011)
Huelva (Spain)	03º15' N, 05º56'W,10 m	Urban industrial	Jan.-Dec. 2009	0.7±0.4	(Reche et al., 2011)
Barcelona (Spain)	02º07'E, 41º23' N, 80 m	Urban background	Jan.-Dec. 2009	1.7±0.6	(Reche et al., 2011)

Table A3. Mean annual ABL heights at different hours of the day and by season (Wi: winter; Sp: spring; Su: summer; Au: autumn; An: annual). Pearson correlations between eBC and ABL heights.

	Mean ABL altitude (m)					eBC concentration (µg m^{-3})					Pearson correlations				
ABL time (UTC)	Wi	Sp	Su	Au	An	Wi	Sp	Su	Au	An	Wi	Sp	Su	Au	An
0000	192	131	84	102	127	0.66	0.34	0.57	0.56	0.53	**-0.49**	**-0.31**	**-0.26**	**-0.42**	**-0.29**
0300	202	121	56	103	120	0.57	0.49	0.71	0.62	0.60	**-0.49**	**-0.25**	**-0.25**	**-0.37**	**-0.25**
0600	183	216	81	84	140	1.45	0.85	0.87	1.40	1.14	**-0.48**	0.03	-0.19	**-0.46**	**-0.20**
0900	424	695	573	229	480	1.27	0.54	0.55	1.09	0.85	**-0.66**	**-0.32**	**-0.41**	**-0.65**	**-0.70**
1200	923	1213	1287	675	1024	0.80	0.43	0.39	0.77	0.59	**-0.52**	**-0.21**	**0.24**	**-0.59**	**-0.58**
1500	958	1458	1915	741	1268	1.19	0.48	0.41	1.41	0.86	**-0.44**	0.06	**0.29**	**-0.57**	**-0.51**
1800	262	424	504	101	322	2.10	0.82	0.85	2.03	1.43	**-0.56**	**-0.34**	**-0.43**	**-0.51**	**-0.51**
2100	227	151	154	103	158	1.15	0.54	0.62	0.91	0.80	**-0.50**	-0.21	-0.17	**-0.52**	**-0.35**

Bold font indicates that the correlation is significant at 95% level.

Table A4. Mean annual ventilation coefficients at different times of the day and by season (Wi: winter; Sp: spring; Su: summer; Au: autumn; An: annual).

	Mean VC (m^2 s^{-1})				
Time (UTC)	Wi	Sp	Su	Au	An
0000	305.4	163.5	13.8	119.6	181.0
0300	368.5	260.4	5.8	141.7	228.4
0600	302.1	271.9	17.8	58.8	190.2
0900	659.5	1193.2	521.4	306.6	669.2
1200	1744.5	2747.2	2067.7	1145.0	1892.3
1500	1998.9	3413.4	3500.3	1278.1	2442.0
1800	444.6	844.1	823.7	116.9	535.7
2100	366.9	229.9	81.9	102.5	229.3

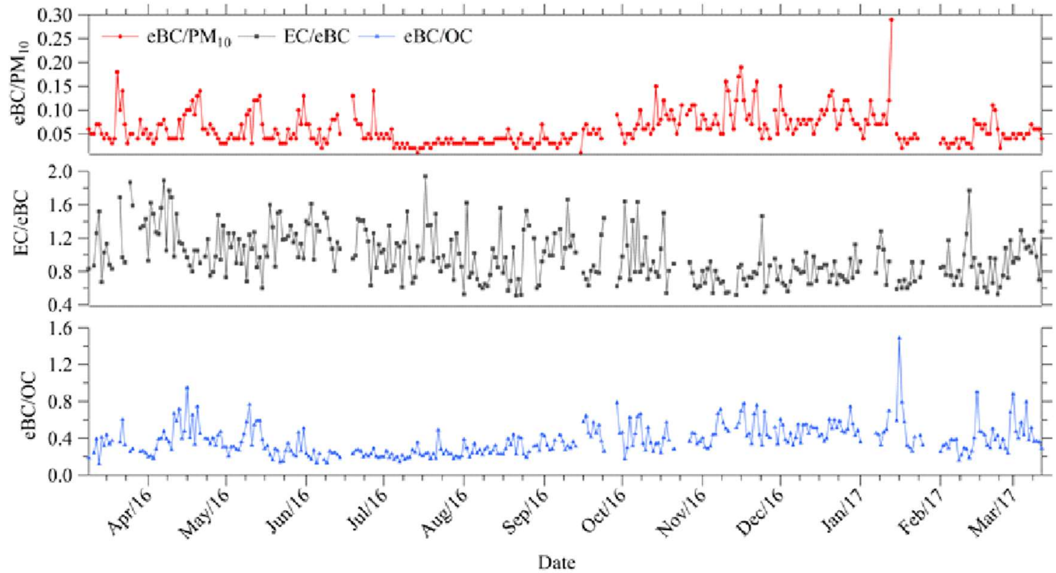

Figure A4. Temporal variations of ratios: eBC /PM_{10} (above), EC/eBC (middle) and eBC/OC (below) at León from January 2016 to March 2017.

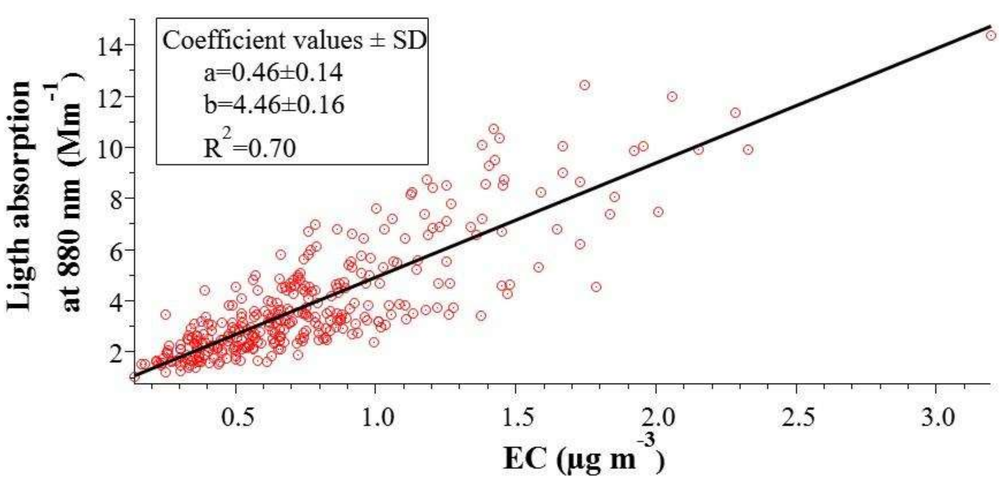

Figure A5. Regression between light absorption at 880 nm estimated from Aethalometer measurements and elemental carbon (EC) measured by TOT method.

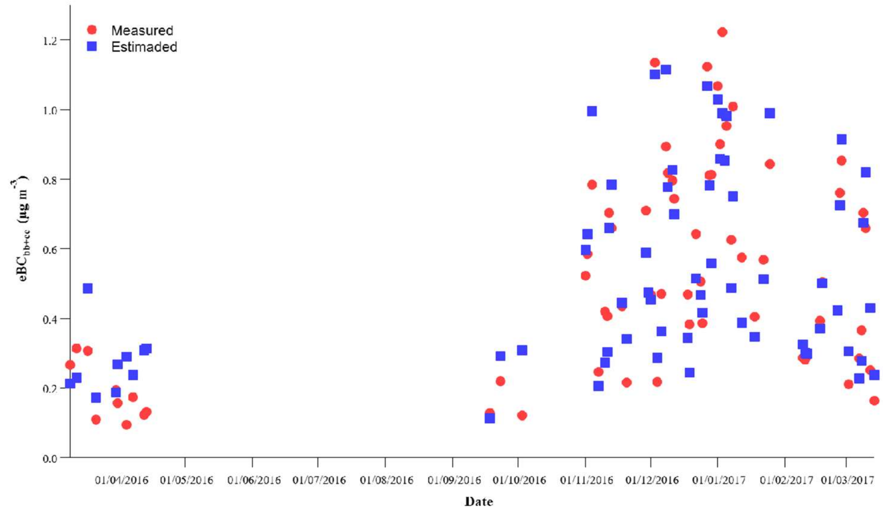

Figure A6. Time series of eBC_{bb+cc} concentration estimated by the model and eBC_{bb+cc} measured at León along sampling campaign.

a)

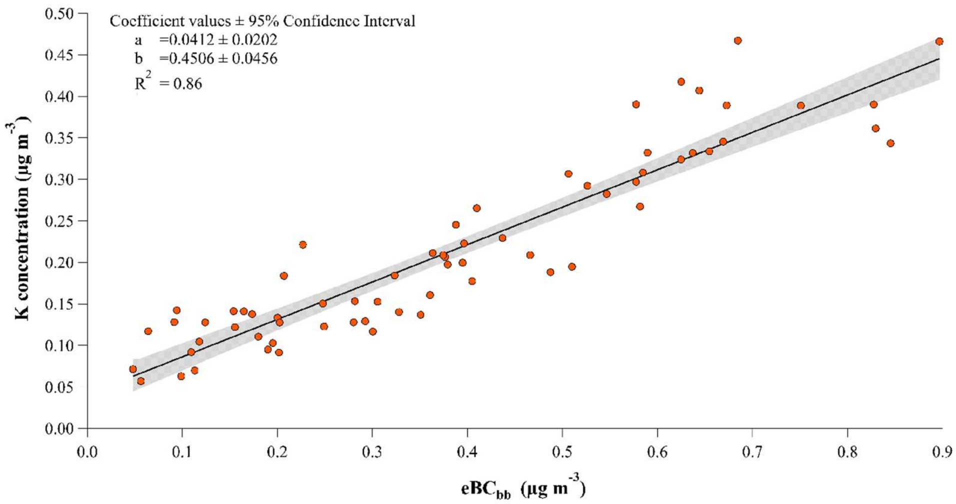

b)

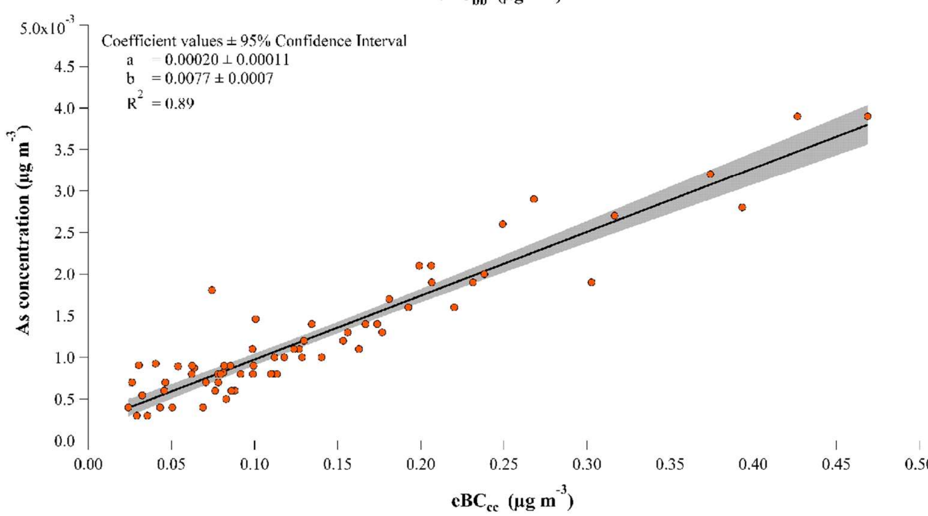

Figure A7. Regression between (a) eBC_{bb}-K and (b) eBC_{cc} –As in the cold period using the whole dataset available.

Table A5. Pearson correlations between eBC, eBC_{ff}, eBC_{bb+cc} concentrations, AAE and meteorological parameters (temperature, relative humidity and wind speed) for monthly and annual analysis.

Parameter		Jan. 16	Feb. 16	Mar. 16	Apr. 16	May. 16	Jun. 16	Jul. 16	Aug. 16	Sep. 16	Oct. 16	Nov. 16	Dec. 16	Jan. 17	Feb. 17	Mar. 17	Annual
T (°C)	eBC	0.048	-0.039	-0.068	-0.036	**0.101**	0.052	**-0.093**	**-0.128**	**0.166**	**0.134**	**0.208**	0.066	0.009	**0.130**	**0.198**	**-0.14**
	eBC_{ff}	**0.086**	0.047	-0.007	0.015	**0.090**	0.046	-0.069	**-0.145**	**0.131**	**0.155**	**0.259**	**0.175**	**0.115**	**0.176**	**0.225**	**-0.04**
	eBC_{bb+cc}	-0.067	**-0.171**	**-0.165**	**-0.175**	**0.090**	0.026	**-0.081**	-0.015	**0.164**	-0.005	0.008	**-0.160**	**-0.182**	-0.003	0.065	**-0.27**
	AAE	**-0.231**	**-0.261**	**-0.211**	**-0.152**	**0.094**	0.009	**-0.116**	**-0.156**	-0.033	-0.042	**-0.319**	**-0.417**	**-0.409**	**-0.130**	**-0.114**	**-0.22**
Wind speed (m s^{-1})	eBC	**-0.367**	**-0.411**	**-0.392**	**-0.274**	**-0.253**	**-0.188**	**-0.245**	**-0.328**	**-0.237**	**-0.261**	**-0.321**	**-0.244**	**-0.346**	**-0.359**	**-0.382**	**-0.31**
	eBC_{ff}	**-0.295**	**-0.313**	**-0.289**	**-0.207**	**-0.211**	**-0.142**	**-0.213**	**-0.324**	**-0.220**	**-0.221**	**-0.213**	**-0.130**	**-0.205**	**-0.228**	**-0.206**	**-0.24**
	eBC_{bb+cc}	**-0.413**	**-0.421**	**-0.414**	**-0.357**	**-0.278**	**-0.144**	**-0.148**	**-0.219**	**-0.158**	**-0.300**	**-0.398**	**-0.346**	**-0.440**	**-0.450**	**-0.459**	**-0.31**
	AAE	-0.075	**-0.137**	-0.073	-0.018	**0.089**	-0.014	-0.047	**-0.139**	**-0.120**	0.044	**-0.288**	**-0.301**	**-0.293**	**-0.088**	**-0.350**	**-0.10**
RH (%)	eBC	**0.216**	0.010	-0.023	**0.135**	0.007	**0.083**	**0.194**	**0.237**	**-0.123**	**-0.145**	-0.021	**-0.161**	**0.224**	**-0.153**	**-0.147**	**0.11**
	eBC_{ff}	**0.178**	-0.020	-0.033	**0.123**	0.035	0.045	**0.164**	**0.254**	**-0.106**	**-0.150**	**-0.079**	**-0.189**	**0.150**	**-0.138**	**-0.118**	**0.07**
	eBC_{bb+cc}	**0.231**	0.057	0.010	**0.109**	**-0.096**	**0.094**	**0.126**	**0.078**	**-0.103**	-0.064	**0.108**	-0.043	**0.255**	**-0.120**	**-0.119**	**0.15**
	AAE	0.052	**0.125**	0.056	**-0.089**	**-0.276**	-0.030	**0.080**	**0.103**	0.063	-0.019	**0.233**	**0.103**	**0.128**	0.036	-0.018	**-0.08**
VC ($m^2 s^{-1}$)	eBC	**-0.268**	**-0.351**	**-0.382**	**-0.238**	**-0.223**	**-0.193**	**-0.246**	**-0.340**	**-0.225**	**-0.254**	**-0.301**	**-0.238**	**-0.331**	**-0.334**	**-0.332**	**-0.268**
	eBC_{ff}	**-0.209**	**-0.277**	**-0.288**	**-0.166**	**-0.188**	**-0.142**	**-0.205**	**-0.345**	**-0.219**	**-0.222**	**-0.211**	**-0.150**	**-0.207**	**-0.225**	**-0.194**	**-0.209**
	eBC_{bb+cc}	**-0.323**	**-0.351**	**-0.381**	**-0.367**	**-0.243**	**-0.156**	**-0.173**	**-0.223**	**-0.140**	**-0.276**	**-0.365**	**-0.300**	**-0.398**	**-0.389**	**-0.362**	**-0.323**
	AAE	**-0.183**	-0.111	-0.068	-0.069	**0.248**	0.000	-.057	**-0.162**	-0.066	0.123	**-0.256**	**-0.247**	**-0.269**	**-0.144**	**-0.287**	**-0.183**

Bold font indicates that the correlation is significant at 95% level

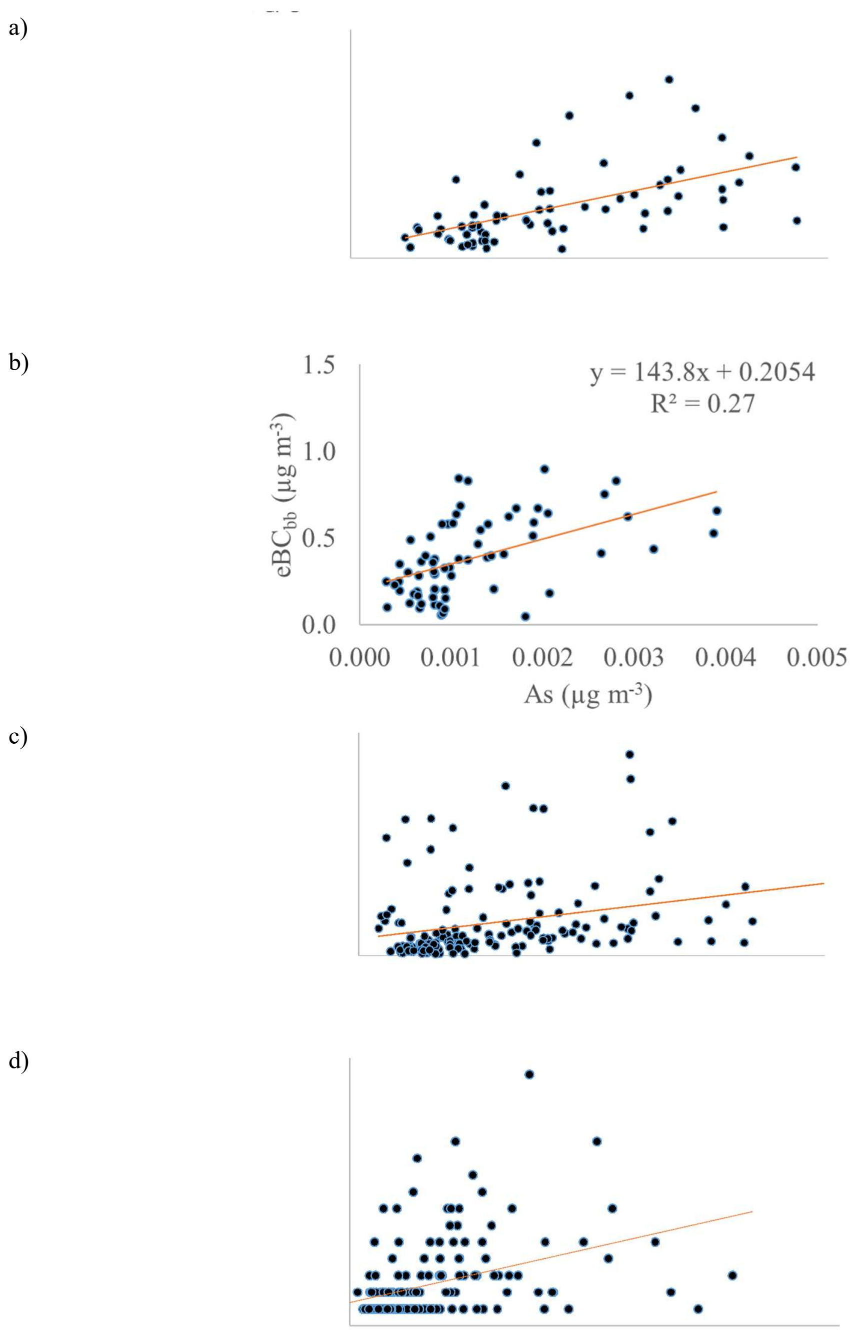

Figure A8. Scatter plot between: (a) eBC_{cc}-K; (b) eBC_{bb} –As; (c) eBC_{bb}-levoglucosan and (d) eBC_{cc}-SO_2 in the cold period.

Table A6. PM_{10} and BC/PM_{10}, OC/EC, EC/BC and BC/OC ratios in León by season for January 2016–March 2017.

Season	PM_{10} (μg m^{-3})	eBC/PM_{10}	OC/EC	EC/eBC	eBC/OC
Cold period	17.0±8.7	0.071±0.036	3.08±1.12	0.86±0.45	0.45±0.17
Warm period	12.6±8.3	0.050±0.029	3.62±1.50	1.09±0.31	0.31±013
Annual	15.6±8.6	0.061±0.034	3.35±1.35	0.98±0.38	0.38±0.17

Table A7. Coefficients, intercept and α value of Kolmogorov-Smirnov (K-S) statistical test for each model built. In N=0, the model obtained with 100% of data is represented.

N	C_K	C_{As}	Intercept	K-S (α)
1	2.08	116.34	-0.069	0.699
2	1.91	119.21	-0.039	0.909
3	1.90	119.47	-0.027	0.454
4	2.13	115.49	-0.076	0.905
5	1.94	138.88	-0.074	0.999
6	1.92	115.61	-0.037	0.905
7	1.90	108.10	-0.028	0.964
8	1.78	153.96	-0.045	0.699
9	1.95	108.37	-0.033	0.905
10	1.95	114.41	-0.039	0.699
0	1.92	119.00	-0.045	0.581

Table A8. Daily Pearson correlations between eBC_{ff}, eBC_{bb}, eBC_{cc} concentrations and meteorological parameters (temperature, relative humidity, wind speed, ventilation coefficient and ABL height) for the cold period.

	T	RH	WS	VC	ABL height
eBC_{ff}	-0.020	**0.202**	**-0.477**	**-0.426**	**-0.505**
eBC_{bb}	**-0.177**	-0.002	**-0.409**	**-0.372**	**-0.501**
eBC_{cc}	**-0.355**	0.107	**-0.369**	**-0.335**	**-0.490**

Bold font indicates that the correlation is significant at 95%.

1. Aethalometer model

Assuming that only two sources exist, the total absorption coefficient $b_{abs,total}$ (λ_w) at wavelength λ_w (Sandradewi et al., 2008) is:

$$b_{abs,total}\,(\lambda_w) = b_{abs,ff}\,(\lambda_w) + b_{abs,bb+}\quad(\lambda_w)$$

where $b_{abs,ff}$ (λ_w), $b_{abs,bb+cc}$ (λ_w) are the absorption coefficients of fossil fuel combustion and biomass burning plus coal combustion, respectively.

Source apportionment of fossil fuel has been estimated through the following equations:

$$\frac{b_{abs,ff(\lambda_1)}}{b_{abs,ff(\lambda_2)}} = \left(\frac{\lambda_{w_1}}{\lambda_{w_2}}\right)^{-AAE_{ff}}$$

$$eBC_{ff} = \frac{b_{abs,ff(\lambda_2)}}{b_{abs,total(\lambda_2)}} \cdot eBC_{total}(\lambda_{w_2})$$

where AAE_{ff} is the absorption Ångström exponent for eBC fossil fuel.

Then, to achieve the aim of estimating the coal combustion (eBC_{cc}) fraction from eBC_{bb+cc}, a model was developed considering the linear regression between eBC_{bb+cc} with biomass (K) and coal (As) combustion tracers, developed in section 3.2 of the paper.

2. Method using the median value to estimate the coal combustion contribution

The days of the cold period (from 15 September to 14 April) with higher As concentration than the median (0.00082 µg m^{-3}) were selected to develop the model. Similar values were obtained than using the method presented in the manuscript, showing the robustness of the model.

The multilinear regression analysis only used these days (N=80) to estimate the model parameters. The estimated eBC_{bb+cc} concentration for biomass burning and coal combustion is expressed as:

$$eBC_{bb+cc}(\mu g\, m^{-3}) = \overbrace{(0.147 \pm 0.047)}^{\approx zero} + \overbrace{(2.02 \pm 0.18) \times C_K}^{eBC_{bb}} + \overbrace{(118 \pm 26) \times C_{As}}^{eBC_{cc}} \qquad \text{Eq. A1}$$

with a model standard error of 0.14 µg m^{-3}, and correlation coefficient of r=0.90.

The application of the model (Eq. A1) allowed the eBC_{cc} and eBC_{bb} to be estimated separately for the cold period. For the days included in the model, the contributions to the eBC_{bb+cc} were broken down into 75% from biomass burning and 25% from coal combustion. After the extraction of eBC_{cc} from eBC_{bb+cc} very strong correlations between eBC_{bb} and K (biomass burning tracer) (r=0.91) and eBC_{cc} and As (coal tracer) (r=0.88) were registered.

The concentrations of EC, segregated by source after application of the model throughout the sampling period, are shown in Table A8 (equivalent to Table 1).

Table A8. Monthly mean values (± standard deviation) calculated for eBC_{ff}, eBC_{bb}, eBC_{cc}, percentage of biomass burning (BB(%)) and coal combustion (CC(%)) from eBC after the application of model.

Year	Season	Month	eBC_{ff} (μg m^{-3})	eBC_{bb} (μg m^{-3})	eBC_{cc} (μg m^{-3})	BB (%)	CC (%)
2016	Winter	January	0.69±0.30	0.31±0.14	0.11±0.05	32±9	11±3
	Winter	February	0.62±0.29	0.31±0.20	0.11±0.07	32±7	11±3
	Spring	March	0.50±0.20	0.20±0.12	0.08±0.04	26±9	11±3
	Spring	April	0.35±0.11	0.12±0.04	0.05±0.02	26±8	12±4
	Spring	May	0.43±0.11	0.13±0.04	-	23±6	-
	Summer	June	0.41±0.14	0.12±0.11	-	22±8	-
	Summer	July	0.41±0.14	0.12±0.10	-	22±8	-
	Summer	August	0.48±0.16	0.12±0.05	-	20±3	-
	Autumn	September	0.58±0.21	0.21±0.15	0.05±0.01	25±8	4±4
	Autumn	October	0.73±0.24	0.23±0.11	0.05±0.02	23±7	6±1
	Autumn	November	0.72±0.34	0.32±0.17	0.09±0.04	29±8	9±2
	Winter	December	1.02±0.36	0.47±0.24	0.17±0.09	28±8	10±3
2017	Winter	January	0.83±0.54	0.55±0.29	0.17±0.11	37±12	11±4
	Winter	February	0.50±0.19	0.28±0.17	0.07±0.04	33±10	9±2
	Spring	March	0.46±0.18	0.31±0.21	0.07±0.04	37±13	8±3

References of Supplementary Material

Costabile, F., Angelini, F., Barnaba, F., Gobbi, G.P., 2015. Partitioning of Black Carbon between ultrafine and fine particle modes in an urban airport vs. urban background environment. Atmos. Environ. 102, 136–144. doi:10.1016/j.atmosenv.2014.11.064

Ji, D., Li, L., Pang, B., Xue, P., Wang, L., Wu, Y., Zhang, H., Wang, Y., 2017. Characterization of black carbon in an urban-rural fringe area of Beijing. Environ. Pollut. 223, 1–11. doi:10.1016/j.envpol.2017.01.055

Joshi, H., Naja, M., Singh, K.P., Kumar, R., Bhardwaj, P., Babu, S.S., Satheesh, S.K., Moorthy, K.K., Chandola, H.C., 2016. Investigations of aerosol black carbon from a semi-urban site in the Indo-Gangetic Plain region. Atmos. Environ. 125, 346–359. doi:10.1016/j.atmosenv.2015.04.007

Klompmaker, J.O., Montagne, D.R., Meliefste, K., Hoek, G., Brunekreef, B., 2015. Spatial variation of ultrafine particles and black carbon in two cities: Results from a short-term measurement campaign. Sci. Total Environ. 508, 266–275. doi:10.1016/j.scitotenv.2014.11.088

Kucbel, M., Corsaro, A., Švédová, B., Raclavská, H., Raclavský, K., Juchelková, D., 2017.

Temporal and seasonal variations of black carbon in a highly polluted European city: Apportionment of potential sources and the effect of meteorological conditions. J. Environ. Manage. 203, 1178–1189. doi:10.1016/j.jenvman.2017.05.038

Liu, D., Allan, J.D., Young, D.E., Coe, H., Beddows, D., Fleming, Z.L., Flynn, M.J., Gallagher, M.W., Harrison, R.M., Lee, J., Prevot, A.S.H., Taylor, J.W., Yin, J., Williams, P.I., Zotter, P., 2014. Size distribution, mixing state and source apportionment of black carbon aerosol in London during winter time. Atmos. Chem. Phys. 14, 10061–10084. doi:10.5194/acp-14-10061-2014

Marín, J.C., Raga, G.B., Arévalo, J., Baumgardner, D., Córdova, A.M., Pozo, D., Calvo, A., Castro, A., Fraile, R., Sorribas, M., 2017. Properties of particulate pollution in the port city of Valparaiso, Chile. Atmos. Environ. 171, 301–316. doi:10.1016/j.atmosenv.2017.09.044

Rattigan, O. V, Civerolo, K., Doraiswamy, P., Felton, H.D., Hopke, P.K., 2013. Long term black carbon measurements at two urban locations in New York. Aerosol Air Qual. Res. 13, 1181–1196. doi:10.4209/aaqr.2013.02.0060

Sandradewi, J., Prévôt, A.S.H., Szidat, S., Perron, N., Alfarra, M.R., Lanz, V.A., Weingartner, E., Baltensperger, U.R.S., 2008. Using aerosol light absorption measurements for the quantitative determination of wood burning and traffic emission contribution to particulate matter. Environ. Sci. Technol. 42, 3316–3323. doi:10.1021/es702253m

Weichenthal, S., Farrell, W., Goldberg, M., Joseph, L., Hatzopoulou, M., 2014. Characterizing the impact of traffic and the built environment on near-road ultrafine particle and black carbon concentrations. Environ. Res. 132, 305–310. doi:10.1016/j.envres.2014.04.007